In Vivo FRET Imaging of Tumor Endothelial Cells Highlights a Role of Low PKA Activity in Vascular Hyperpermeability

(腫瘍内皮細胞の生体内FRETイメージングは血管透過性亢進における低PKA活性の役割を明らかにする)

山内　文生

掲載雑誌 Cancer Research
第76巻 第18号 5266頁～5276頁掲載
平成28年9月15日発行

主論文

In vivo FRET imaging of tumor endothelial cells highlights a role of low PKA activity in vascular hyperpermeability

Fumio Yamauchi[1,2], Yuji Kamioka[1,3], Tetsuya Yano[2], Michiyuki Matsuda[1]

[1]Department of Pathology and Biology of Diseases, Graduate School of Medicine, Kyoto University; [2] Medical Imaging System Development Center, R&D Headquarters, Canon Inc.; [3]Innovative Techno-Hub for Integrated Medical Bio-Imaging, Kyoto University.

Running title: Endothelial hyperpermeability and low PKA activity in tumors

Key words: Vascular hyperpermeability, Tumor endothelial cells, PKA, Förster resonance energy transfer (FRET), In vivo imaging (5 keywords)

Grant Support: M. Matsuda was funded by the Innovative Techno-hub for Integrated Medical Bio-imaging Project of MEXT, by the Platform Project for Supporting in Drug Discovery and Life Science Research (Platform for Dynamic Approaches to Living System) of MEXT and AMED, Japan, by a Grant-in-Aid for Scientific Research on Innovative Areas "Resonance Biology" of MEXT, and by the Naito Foundation.

Corresponding Author: Michiyuki Matsuda, Department of Pathology and Biology of Diseases, Graduate School of Medicine, Kyoto University, Yoshida-Konoe-Cho, Sakyo-ku, Kyoto 606-8501, Japan. Phone: 81-75-753-4421; Fax: 81-75-753-4655; E-mail: matsuda.michiyuki.2c@kyoto-u.ac.jp

Conflict of interest: Fumio Yamauchi and Tetsuya Yano are employees of Canon Inc., Japan.

Notes: This manuscript consists of a main text containing 6,000 words, 7 figures.

Abstract

Vascular hyperpermeability is a pathological hallmark of cancer. Previous in vitro studies have elucidated roles of various signaling molecules in vascular hyperpermeability; however, the activities of such signaling molecules have not been examined in live tumor tissues for technical reasons. Here, by in vivo two-photon excitation microscopy with transgenic mice expressing biosensors based on Förster resonance energy transfer (FRET), we examined the activity of protein kinase A (PKA), which maintains endothelial barrier function. The level of PKA activity was significantly lower in the intratumoral endothelial cells than the subcutaneous endothelial cells. PKA activation with a cAMP analog alleviated the tumor vascular hyperpermeability, suggesting that the low PKA activity in the endothelial cells may be responsible for the tumor-tissue hyperpermeability. Because the vascular endothelial growth factor (VEGF) receptor is a canonical inducer of vascular hyperpermeability and a molecular target of anti-cancer drugs, we examined the causality between VEGF receptor activity and the PKA activity. Motesanib, a kinase inhibitor for VEGF receptor, activated tumor endothelial PKA and reduced the vascular permeability in the tumor. Conversely, subcutaneous injection of VEGF decreased endothelial PKA activity and induced hyperpermeability of subcutaneous blood vessels. Notably, in cultured human umbilical vascular endothelial cells, VEGF activated PKA rather than decreasing its activity, highlighting the remarkable difference between its actions in vitro and in vivo. These data suggested that the VEGF receptor signaling pathway increases vascular permeability, at least in part, by reducing endothelial PKA activity in the live tumor tissue.

Introduction

Blood vessels in tumors are significantly different from those in normal tissues in terms of structure and function (1). For example, vascular permeability is markedly increased in tumor tissues, and this increase is associated with angiogenesis and metastasis (2-6). Accordingly, suppression of the vascular permeability results in the inhibition of tumor growth and metastasis (7).

The high vascular permeability in tumor tissues is caused by various factors including the structural abnormality of blood vessels (2, 8), pressure or concentration gradients between compartments, and the properties of endothelial cells and/or pericytes (2, 6). Among a number of molecules that regulate blood vessels in tumor tissues, vascular endothelial growth factor (VEGF) has been a focus of intensive research (6, 9). VEGF increases vascular permeability by promoting transcytosis (10-14) and enlarging the intercellular gaps of endothelial cells (15). The inhibition of VEGF and VEGF receptors (VEGFRs) results in a decrease of permeability and the normalization of tumor vasculature, which in turn results in the inhibition of tumor growth and improvement of anti-cancer chemotherapy (7).

The VEGF-induced increase in vascular permeability is mediated by various intracellular signaling pathways, including those of PTPs, Src, PI3K, uPA, PLC-γ, and eNOS (6). Another signaling molecule that has been shown to regulate vascular permeability is cAMP. In microvascular endothelial cells, cAMP mediates endothelial barrier function by suppressing vascular permeability (16, 17). Further studies have shown that increased cAMP triggers sequential activation of protein kinase A (PKA), a guanine nucleotide exchange factor Tiam1, and a small GTPase Rac1, resulting in an increase in barrier function (18, 19). On the other hand, cAMP can also contribute to the endothelial barrier function via cAMP-dependent guanine nucleotide exchange factor Epac/cAMP-GEF and a small GTPase Rap1 (20, 21). Notably, the contribution of these potential effectors downstream of VEGFR to the hyperpermeability in tumor tissue has not been assessed in live tissues.

Visualization of tumor tissues by two-photon excitation microscopy has opened new windows into the dynamics of angiogenesis and the involvement of hematopoietic cells in

tumorigenesis (22, 23). Meanwhile, using cancer cells expressing Förster resonance energy transfer (FRET) biosensors, the effects of anti-cancer drugs on the target molecules have been visualized in the xenograft/homograft recipient mice, revealing considerable heterogeneity among cancer cells (24, 25). To conduct similar approaches for the host cells, transgenic mice expressing the FRET biosensors are needed. We and other have developed such transgenic mice, collectively designated FRET mice, for the visualization of activities of protein kinases and small GTPases (26, 27). Here, by in vivo FRET imaging of the intratumoral blood vessels, we show that the basal activity of tumor endothelial PKA is significantly lower than that of normal endothelial cells and that the cAMP analog could alleviate the increased vascular permeability in the tumors.

Materials and Methods

Cells and reagents

Panc-02 mouse pancreatic cancer cells were obtained from NIH (Bethesda, MD). B16-F10 mouse melanoma cells were obtained from the American Tissue Culture Collection (ATCC; Manassas, VA). Primary human vascular endothelial cells (HUVEC) were purchased from the Lonza Group, Ltd. (Basel, Switzerland). These cell lines were acquired after 2012. Frozen stocks were prepared from initial stocks, and within every 2 months, a new frozen stock was used for the experiments. Colon-38 mouse colon cancer cells and 3LL mouse lung carcinoma cells were provided by Drs. Setoyama and Chiba at Kyoto University and Drs. Shime and Seya at Hokkaido University, respectively, and periodically authenticated by morphologic inspection. Tumor or normal endothelial cells were isolated from FRET mice as described previously (28). A pCX4 retroviral vector was used to express the Keima fluorescent protein or the Epac-cAMP sensor (29, 30). Cancer cells and HUVEC were maintained in DMEM containing 10% fetal bovine serum and in EGM-2MV media (Lonza), respectively. Following reagents were used: Motesanib (Selleck Chemicals, Houston TX, USA), Qtracker 655 (Thermo Fisher Scientific Inc, Waltham, MA), N^6,2'-O-dibutyryladenosine 3',5'-cyclic monophosphate sodium salt (Daiichi Sankyo Company, Ltd., Tokyo, Japan), 8-(4-chlorophenylthio)-2′–O-methyladenosine 3′,5′-cyclic monophosphate (007) and N^6-benzoyladenosine-3′,5′-cyclic monophosphate (6-Bnz) (Biolog Life Science Institute, Bremen, Germany), Evans blue and isoflurane (Wako Pure Chemicals, Ltd., Osaka, Japan), Mouse VEGF164 (BioLegend, San Diego, CA), H89 and PD0325901 (Sigma-Aldrich Co. LLC).

Mice and tumor implantation

We used PKAchu mice expressing the PKA FRET biosensor AKAR3EV-NES, PKA-NC mice expressing a negative control FRET biosensor AKAR3EV-NC, and Eisuke mice expressing the ERK FRET biosensor EKAREV-NES (26). FRET mice were back-crossed more than nine generations to C57BL/6N Jcl mice (Japan SLC Inc., Shizuoka, Japan). Cancer

cells (2 x10^6 cells/50 μL PBS) were injected subcutaneously into the flanks of mice. The animal protocols were reviewed and approved by the Animal Care and Use Committee of Kyoto University Graduate School of Medicine (Nos. 12064, 13074, 14079, and 15064).

Two-photon excitation microscopy and image processing

We used an FV1000MVE inverted microscope (Olympus Corporation, Tokyo, Japan) equipped with a 30 x 1.05NA silicon-immersion objective lens (UPLSAPO 30xS; Olympus), and an InSight DeepSee Ultrafast laser (0.95 W at 900 nm, Spectra Physics, Mountain View, CA). The excitation wavelength for cyan fluorescent protein (CFP) was 840 nm. For more information, refer to supplementary materials and methods. Acquired images were processed and analyzed with MetaMorph software (Molecular Devices, Sunnyvale, CA) as described previously (26, 31).

In vivo observation of the vascular endothelial cells

Mice were anesthetized with 1.5–2% isoflurane inhalation and placed in the prone position. Skin flap was then placed on a cover-glass. As controls, subcutaneous capillaries with a diameter of less than 15 μm and subcutaneous arterioles or venules from 15 to 50 μm in diameter were also observed in each experiment. Images were acquired every 2 or 4 min at a scan speed of 2 μs/pixel. During imaging, reagents were administered in 100 μL PBS via the orbital plexus, if necessary: Motesanib (50 mg/kg), VEGF164 (5 μg/mouse), dbcAMP (50 mg/kg), 6-Bnz (50 mg/kg), 007 (50 mg/kg), and Qtracker 655 (5 μL/mouse). Images of the FRET/CFP ratio as an index of PKA or ERK activity were prepared as described in the supplementary materials and methods (32).

To visualize endothelial PKA activity under VEGF stimulation, mouse VEGF164 (400 ng in 50 μL PBS) was injected intradermally 30 min before observation. To examine PKA activity under the specific inhibitor treatment, H89 (5 mM in 50 μL of 5% DMSO/saline) or vehicle (5% DMSO/saline) was added to the surface of Colon-38 tumors on the PKAchu mice.

Vascular permeability assays (modified Miles assays)

Evans blue (10 mg/mL in PBS) was injected intravenously into tumor-bearing C57BL/6N Jcl mice at a concentration of 50 mg/kg with or without following reagents: dbcAMP (50 or 100 mg/kg), 007 (10, 25 or 50 mg/kg), 6-Bnz (10, 25 or 50 mg/kg) or Motesanib (50 mg/kg). Mice were subjected to PBS perfusion 2 hr after the dye injection and sacrificed. The tumor and skin were then excised, dried at 60°C for 24 hr, and weighed. The dye was extracted from the tissues by incubation with 0.5 ml *N,N*-dimethylformamide (Nacalai Tesque Inc., Kyoto, Japan) at 56°C for 48 hr. The dye was quantified by measuring the absorbance at 620 nm. The extracted dye was normalized to nanograms dye per milligram tumor dry weight. In some experiments, 30 min after Evans blue injection, 400 ng mouse VEGF164 in 50 μL PBS was injected subcutaneously.

FRET imaging of PKA, ERK, or Epac activity in HUVEC

Lenti-X™ 293T cells (Takara Bio Inc., Shiga, Japan) were cotransfected with the pCSIIbsr vector encoding the FRET biosensors AKAR3EV-NES or EKAREV-NES, psPAX2 (Addgene, Cambridge, MA), and pCMV-VSV-G-RSV-Rev by using 293fectin (Thermo Fisher Scientific Inc.). HUVEC were infected with the resulting lentivirus and cultured with EGM-2MV media on cover glass-bottomed dishes for 16–24 hr before imaging. CFP and YFP images of HUVEC were obtained by using an inverted microscope (LCV110; Olympus). Cells were stimulated with vehicle (PBS), VEGF164 (50-100 ng/mL), PD0325901 (10 μM) and Forskolin (50 μM) - IBMX (500 μM) and analyzed as described previously (31).

Immunohistochemistry

Formalin-fixed tissue sections were incubated with primary antibodies to CD31 (ad22538; Abcam, Cambridge, UK), GFP (JL-8; Takara Bio Inc.), VEGFR2 (55B11; Cell Signaling Technology) or pVEGFR2 (19A10; Cell Signaling Technology) followed by incubation with secondary antibodies (Alexa Fluor; Thermo Fisher Scientific Inc.). Anti-CD31 antibody

conjugated with Alexa Fluor 594 (BioLegend), Hoechst33258, or DAPI (Sigma-Aldrich Co. LLC, USA) was also used.

Statistical analysis

All data were expressed as means ± standard deviation (SD). Statistical analysis was performed using GraphPad Prism software (GraphPad Software Inc.). Student's *t*-test and one-way ANOVA with Tukey post hoc analysis were used to determine statistically significant differences. *P* values < 0.05 were considered to indicate statistical significance. *P < 0.05; **P < 0.01; ***P < 0.001.

Results

In vivo imaging of tumor-bearing FRET mice visualized the PKA activity in the vascular endothelial cells of tumor and subcutaneous tissue.

To understand the roles played by PKA in the hyperpermeability of intratumoral blood vessels, we compared the endothelial PKA activities between normal subcutaneous blood vessels and intratumoral blood vessels. For visualization of the PKA activity in the tumor-bearing mice (TBM), we used PKAchu mice, which expressed a cytoplasmic FRET biosensor for PKA. The structure, mode of action, and stability of the FRET biosensors have been described previously (26, 33). Briefly, phosphorylation of the substrate domain of the FRET biosensor increases in the FRET signal, which can be quantified by the intensity ratio of 530 nm FRET channel over 475 nm CFP channel (Supplementary Fig.S1A-C). Syngeneic Colon-38 colon cancer cells that expressed the Keima fluorescent protein were subcutaneously implanted in the flanks of the PKAchu mice. After tumor cells grew to palpable sizes, tumors and subcutaneous tissues exposed by the skin-flap method were observed under an inverted two-photon excitation microscope (Fig. 1A). In the tumor tissue, the FRET biosensor-expressing host cells, such as vascular endothelial cells and inflammatory cells were clearly distinguished from the Keima-expressing Colon-38 cancer cells (Fig. 1B, left). In the subcutaneous tissue of TBM, capillaries were clearly detected among the dense collagen fibers (Fig 1B, right).

The PKA activity of host cells is represented by FRET/CFP ratio images (Fig. 1C). The ratio range was fixed from 0.8 to 1.8 for consistency. As shown in the enlarged image, the PKA activity in the intratumoral endothelial cells was lower than the PKA activity in the subcutaneous endothelial cells (Fig. 1C). The PKA activity of neutrophils and platelets in the vessels could be conveniently used as internal controls (Fig. 1C, arrows): The FRET/CFP values of neutrophils and platelets in the intratumoral blood vessel and subcutaneous capillary were 1.37 ± 0.15 ($n = 6$) and 1.30 ± 0.07 ($n = 6$), respectively. We identified endothelial cells primarily by the location and shape of cells (Supplementary Fig.S1D). If necessary, Z-stack images and images of Qtracker 655 vascular tracer were used to distinguish endothelial cells

from other cells such as pericytes (Supplementary Fig.S1E-G). Furthermore, we confirmed that the GFP-positive cells lining the internal surface of intratumoral blood vessels were positive for anti-CD31 antibody (Fig. 1D).

To verify the specificity of the biosensor, we performed in vivo FRET imaging with a PKA inhibitor, H89, a PKA-specific agonist, 6-Bnz, or an Epac/cAMP-GEF specific-agonist, 007 (Supplementary Fig.S2). H89 robustly reduced PKA activity in stromal cells and slightly in the tumor endothelial cells (Supplementary Fig.S2A, B). As expected, 6-Bnz, but not 007, activated PKA in tumor endothelial cells (Supplementary Fig.S2C).

The PKA activity of intratumoral endothelial cells was lower than that of subcutaneous endothelial cells.

Encouraged by the findings obtained using Colon-38 cells, we extended our approach by using other cancer cells with different morphological features (Fig. 2A). Because of the small cytoplasmic area of endothelial cells in the tangential image, the signal-to-noise ratios of FRET images were lower than those for the other cell types. Therefore, we time-lapse-imaged and quantified the PKA activity of at least 17 endothelial cells of more than three mice under each condition (Fig. 2B). The PKA activity was significantly lower in the tumor endothelial cells of all four cell lines examined—Colon-38 (colon cancer), Panc-02 (pancreatic cancer), B16-F10 (melanoma), and 3LL (lung cancer)—than in all normal endothelial cells of TBM and control mice. We did not find a significant difference in the PKA activity among the endothelial cells of arterioles, capillaries, and venules. We also failed to detect any difference between the subcutaneous endothelial cells in TBM and control mice. Notably, the densities of tumor cells, host cells, blood vessels, and collagen fibers were quite divergent among the tumors, strongly suggesting that the low PKA activity is a primary characteristic of the nascent intratumoral endothelial cells. To exclude the possibility that the difference in the FRET signal between the intratumoral and subcutaneous endothelial cells was caused by the difference in the physical properties of tumor tissues and subcutaneous tissues, we performed similar experiments with the PKA-NC mice, which expressed a negative control PKA FRET biosensor lacking the PKA

phosphorylation site in the same FRET biosensor backbone. No significant differences were observed between the intratumoral and subcutaneous endothelial cells of PKA-NC mice (Fig. 2C). These data strongly argued for the low intratumoral endothelial PKA.

No significant differences in ERK activities were observed between intratumoral and subcutaneous tissues.

We extended the same approach to Eisuke mice, which are transgenic mice expressing a FRET biosensor for ERK (Fig. 3 and Supplementary Fig.S1A, C). The distribution of ERK activity among different endothelial cells was not significantly different from that of PKA activity shown in Fig. 2. Nevertheless, we failed to detect significant difference in ERK activity between the intratumoral and subcutaneous endothelial cells. We also observed no difference between the tumor-bearing mice and control mice. These observations indicated that the difference between tumor tissue and subcutaneous tissue was specific for PKA activity.

dbcAMP decreased the vascular permeability and increased the endothelial PKA activity in tumor tissues.

Previous studies have demonstrated that endothelial PKA is a key player for endothelial barrier function (18, 19). It is also known that vascular permeability is high in intratumoral blood vessels. Therefore, we hypothesized that the low PKA activity in the intratumoral endothelial cells is responsible for the high vascular permeability in the tumor. To validate this hypothesis, we conducted a modified Miles assay for measuring vascular permeability in the presence or absence of a cAMP analog, dbcAMP (Fig. 4A).

Colon-38 or Panc-02 cells were injected into the flanks of C57BL/6N Jcl mice to prepare TBM. After intravenous injection of Evans blue to TBM, the dye extravasation from the tumor and the skin was quantified at 2 hr post-administration (Fig. 4A). As expected, in the PBS-injected Colon-38-bearing mice the extravasation of Evans blue dye was higher in the tumor than the skin, confirming the hyperpermeability of the tumor vessels (Fig. 4B). In the dbcAMP-injected mice, however, the extravasation of Evans blue was as low as that in the skin.

Importantly, the effect of dbcAMP was not detectable in the skin, strongly suggesting that the PKA activity in the normal subcutaneous endothelium is sufficiently high to prevent extravasation of Evans blue. Similar results were obtained with the Panc-02 tumor model. The effect of administered dbcAMP on the endothelial PKA was validated by in vivo FRET imaging (Fig. 4C). dbcAMP robustly activated PKA in both tumor and normal endothelial cells (Fig. 4D). Taken together, these data indicate that tumor vascular permeability is in part dependent on the low endothelial PKA activity.

Not only PKA but also Epac/cAMP-GEF reduced tumor vascular permeability.

cAMP can regulate vascular permeability by PKA and Epac/cAMP-GEF. To assess the contribution of PKA and Epac/cAMP-GEF to the cAMP-induced decrease of tumor vascular permeability, we used a PKA-specific agonist, 6-Bnz, and an Epac/cAMP-GEF specific-agonist, 007. Mice were injected intravenously together with Evans blue dye and the agonists (10, 25 and 50 mg/kg) and subjected to a Miles assay (Fig. 5). Both 6-Bnz and 007 decreased the extravasation of Evans blue in a dose-dependent manner. Neither dbcAMP nor 007 significantly affected the extravasation of Evans blue in the skin. Although we did not test the cAMP levels in the endothelial cells, these data strongly suggested that the low cAMP level in tumor endothelial cells at least partially contributed to the high vascular permeability in tumor tissues.

Inhibition of VEGFR activated tumor endothelial PKA and reduced vascular permeability in tumor tissue.

The cAMP level and PKA activity are regulated by numerous signaling molecules, including Gs-coupled GPCRs and phosphodiesterases (34). Therefore, rather than examining the contribution of direct regulators of cAMP, we focused on vascular endothelial growth factors (VEGFs) and their cognate receptors (VEGFRs), which have been shown to play key roles in vascular permeability and angiogenesis in tumors (6). To examine the role of VEGFR signaling on PKA, we tested the effect of a VEGFR inhibitor on tumor vascular permeability

and endothelial PKA activity by Miles assay and in vivo FRET imaging, respectively. Among the available VEGFR kinase inhibitors, we chose Motesanib based on its high water solubility. Mice were injected intravenously with Evans blue dye and Motesanib (50 mg/kg) and subjected to the Miles assay. Motesanib reduced the extravasation of Evans blue in the tumor, but not the skin, indicating that Motesanib inhibited tumor vascular permeability (Fig. 6A). This finding is consistent with previous studies that demonstrated an inhibition of VEGF-induced vascular permeability by Motesanib administration (35). By immunohistochemistry, we confirmed that Motesanib suppressed the VEGFR2 tyrosine kinase activity, but not the expression of VEGFR2 (Supplementary Fig.S3).

We next examined the response of endothelial PKA activity to Motesanib by in vivo FRET imaging. Motesanib robustly activated PKA in the endothelial cells of the tumors, but not in the endothelial cells of the subcutaneous tissues (Fig. 6B), indicating that VEGFR played a major role in the suppression of PKA. Notably, Motesanib had no effect on the ERK activities in tumor and normal endothelial cells (Fig. 6C). The lack of effect on ERK activity is probably due to the low basal ERK activity. In fact, when ERK activity in tumor endothelial cells was elevated by VEGF, Motesanib markedly decreased ERK activity (Supplementary Fig.S4A-C).

VEGF decreased endothelial PKA activity and increased vascular permeability in vivo.

To confirm the role of PKA on the VEGF-induced increase in vascular permeability, PKA activity and vascular permeability were measured in the VEGF-administered skin. Evans blue was intravenously injected and 30 min later, PBS or VEGF164 was injected intradermally. VEGF increased the vascular permeability in the skin (Fig. 7A). In a parallel experiment, PBS or VEGF164 was intradermally injected into PKAchu mice, followed by in vivo FRET imaging for PKA activity (Fig. 7B). As shown in Figure 7C, the PKA activity in the capillary endothelial cells was significantly lower in the VEGF-injected skin than in the PBS-injected skin. Taken together, these data strongly suggested that the VEGFR signaling pathway increases vascular permeability in part by reducing the PKA activity in endothelial cells.

Finally, we attempted to recapitulate the VEGF-induced decrease of PKA activity in human umbilical vascular endothelial cells (HUVEC) expressing the PKA FRET biosensor. In stark contrast to our in vivo observations, we found that PKA activity was increased rapidly in HUVEC (Fig. 7D, 7E). The increase in cAMP level was also confirmed by Epac-cAMP sensor (Supplementary Fig.S5) (29). To examine if the discrepancy was caused by the in vitro experimental condition, we isolated intratumoral and subcutaneous endothelial cells from the transgenic and repeated the experiments (Supplementary Fig.S6). In contrast to HUVEC and similarly to the subcutaneous endothelial cells, the PKA activity in the isolated subcutaneous endothelial cells was higher than the isolated intratumoral endothelial cells and decreased by VEGF stimulation. These results suggest that the isolated primary cells are more similar to the vascular endothelial cells in vivo than to the cultured HUVEC. This is likely due to the difference in proliferation ability between the two types of normal endothelial cells. In fact, the isolated endothelial cells ceased proliferation and became senescent several days after isolation.

Discussion

Intratumoral vascular hyperpermeability regulates tumor progression, tumor metastasis, and intratumoral drug delivery (5). Although inhibition of PKA is known to increase vascular permeability in normal tissue (36), the role of PKA in the intratumoral vascular hyperpermeability has not been clarified. Our in vivo FRET imaging has implied that the basal PKA activity is significantly lower in the intratumoral endothelial cells than in the subcutaneous endothelial cells (Fig. 2B) and that the low PKA activity may be responsible for the intratumoral vascular hyperpermeability. Due to the technical difficulties, we needed to observe implanted cancer cells that grow faster than naturally-occurring cancer cells. It awaits further study whether this property is a common hallmark of cancer cells.

VEGF-mediated activation of endothelial VEGFRs is a canonical pathway to increase vascular permeability in diseased tissues, including tumors (35, 37). Accordingly, we observed that VEGF increased the vascular permeability of subcutaneous tissue (Fig. 7A), while a VEGFR inhibitor, Motesanib, reduced the vascular permeability of tumor tissue (Fig. 6A). Importantly, under both conditions, PKA activity in the endothelial cells was inversely correlated with the vascular permeability. In contrast to our observations, Xiong et al. have shown that VEGF increases cAMP and activates PKA in HUVEC (38). We have also confirmed that VEGF activates PKA in HUVEC (Fig. 7D, 7E). In vivo environmental factors, such as cytokines, growth factors, extracellular matrix, or 3D structures including an interaction with pericytes, may account for this discrepancy between the in vivo and in vitro observations. For example, two VEGFR-family proteins, VEGFR1 and VEGFR2, are localized at the apical and basolateral surfaces of endothelial cells, respectively, in the tissues (39); therefore, when VEGF is secreted by the interstitial cells, VEGFR2, but not VEGFR1, will primarily transduce signals in the diseased tissues. VEGFR2 may suppress, rather than activate, PKA in vivo. In contrast, VEGF will stimulate both VEGFR1 and VEGFR2 in vitro and activate PKA.

How is PKA activity regulated in the normal and intratumoral endothelial cells? In most cell types, PKA activity depends exclusively on the cAMP level (40). Therefore, the

endothelial PKA activity may be regulated primarily by the activity of G-protein coupled receptors (GPCRs) associated with either Gs or Gi. Previous studies have demonstrated specific expression of Gi–coupled receptors such as the Apelin receptor (41) and sphingosine-1-phosphate receptors (42) in tumor endothelial cells. An endogenous PKA inhibitor (PKI) may also be involved in the regulation of PKA (16). It is important to note that not only the authentic ligand to GPCR but also other receptors such as VEGFR can regulate the activity of GPCR. Needless to say, we cannot exclude the possible involvement of other cAMP regulators from the regulation of cAMP level and PKA activity in the endothelial cells. For example, phosphodiesterases have been shown to regulate cAMP level and PKA activity under various conditions (34). Further studies will be required to elucidate the signaling pathway by which cAMP and PKA activity in the intratumoral endothelial cells are controlled and in turn control the permeability of endothelial cells.

cAMP stabilizes the endothelial barrier and antagonizes the cytokine-mediated increase of vascular permeability (17, 20). To examine which cAMP effector plays a principal role in the maintenance of endothelial barrier function, we used specific activators for PKA and Epac/cAMP-GEF. Unexpectedly, we found that both the PKA-specific activator 6-Bnz and the Epac/cAMP-GEF-specific activator 007 decreased the vascular permeability of tumor tissues (Fig. 5), suggesting that the endothelial barrier is maintained by both PKA and Epac/cAMP-GEF in vivo. Our results also underscored that in vivo FRET imaging can help not only to clarify biological processes, but also in the search for new strategies of anti-cancer therapy. Previous studies demonstrated that inhibition of tumor vascular permeability could lead to suppression of tumor growth (43) and improvement of chemotherapy (44). Taken these observations into account, by restoring PKA activity in the intratumoral endothelial cells to the level in normal endothelial cells, the intratumoral vascular hyperpermeability may be alleviated and thereby control tumor growth.

A drawback of the in vivo FRET imaging is that validation of the specificity is not as easy as in studies by using tissue culture cells. For example, we cannot exclude the possibility that the PKA biosensor is also phosphorylated by other kinases, unless we use PKA knock out

mice. Similarly, because of the specificity issue (45), the H89-induced decrease in FRET signal (Supplementary Fig. 2) may not be sufficient for excluding the involvement of other kinases in the high basal FRET signal in normal endothelial cells. Nevertheless, we conclude that in vivo FRET imaging is a powerful approach to fill the gap between in vitro signal transduction research and in vivo cancer biology, if we understand the limitation of this technology.

Acknowledgments

We are grateful to Kees Jalink for Epac cAMP-sensor, Shigetomo Fukuhara for insightful suggestions and the members of the Matsuda Laboratory for their helpful input, Y. Inaoka, K. Hirano, K. Takakura and A. Kawagishi for their technical assistance, and Medical Research Support Center of Kyoto University for in vivo imaging.

References

1. McDonald DM, Baluk P. Significance of blood vessel leakiness in cancer. Cancer research. 2002;62:5381-5.
2. Gerlowski LE, Jain RK. Microvascular permeability of normal and neoplastic tissues. Microvasc Res. 1986;31:288-305.
3. Maeda H, Fang J, Inutsuka T, Kitamoto Y. Vascular permeability enhancement in solid tumor: various factors, mechanisms involved and its implications. International Immunopharmacology. 2003;3:319-28.
4. Mehta D, Malik AB. Signaling mechanisms regulating endothelial permeability. Physiol Rev. 2006;86:279-367.
5. Azzi S, Hebda JK, Gavard J. Vascular permeability and drug delivery in cancers. Front Oncol. 2013;3:211.
6. Weis SM, Cheresh DA. Pathophysiological consequences of VEGF-induced vascular permeability. Nature. 2005;437:497-504.
7. Jain RK. Antiangiogenesis strategies revisited: from starving tumors to alleviating hypoxia. Cancer Cell. 2014;26:605-22.
8. Yuan F, Dellian M, Fukumura D, Leunig M, Berk DA, Torchilin VP, et al. Vascular permeability in a human tumor xenograft: molecular size dependence and cutoff size. Cancer research. 1995;55:3752-6.
9. Jain RK. Normalizing tumor vasculature with anti-angiogenic therapy: a new paradigm for combination therapy. Nat Med. 2001;7:987-9.
10. Roberts WG, Palade GE. Increased microvascular permeability and endothelial fenestration induced by vascular endothelial growth factor. J Cell Sci. 1995;108 (Pt 6):2369-79.
11. Feng D, Nagy JA, Brekken RA, Pettersson A, Manseau EJ, Pyne K, et al. Ultrastructural localization of the vascular permeability factor/vascular endothelial growth factor (VPF/VEGF) receptor-2 (FLK-1, KDR) in normal mouse kidney and in the

hyperpermeable vessels induced by VPF/VEGF-expressing tumors and adenoviral vectors. J Histochem Cytochem. 2000;48:545-56.

12. Hobbs SK, Monsky WL, Yuan F, Roberts WG, Griffith L, Torchilin VP, et al. Regulation of transport pathways in tumor vessels: role of tumor type and microenvironment. Proc Natl Acad Sci U S A. 1998;95:4607-12.
13. Hippenstiel S, Krull M, Ikemann A, Risau W, Clauss M, Suttorp N. VEGF induces hyperpermeability by a direct action on endothelial cells. Am J Physiol. 1998;274:L678-84.
14. Gavard J, Gutkind JS. VEGF controls endothelial-cell permeability by promoting the beta-arrestin-dependent endocytosis of VE-cadherin. Nat Cell Biol. 2006;8:1223-34.
15. Monsky WL, Fukumura D, Gohongi T, Ancukiewcz M, Weich HA, Torchilin VP, et al. Augmentation of transvascular transport of macromolecules and nanoparticles in tumors using vascular endothelial growth factor. Cancer research. 1999;59:4129-35.
16. Lum H, Jaffe HA, Schulz IT, Masood A, RayChaudhury A, Green RD. Expression of PKA inhibitor (PKI) gene abolishes cAMP-mediated protection to endothelial barrier dysfunction. Am J Physiol. 1999;277:C580-8.
17. Irie K, Fujii E, Ishida H, Wada K, Suganuma T, Nishikori T, et al. Inhibitory effects of cyclic AMP elevating agents on lipopolysaccharide (LPS)-induced microvascular permeability change in mouse skin. Br J Pharmacol. 2001;133:237-42.
18. Waschke J, Drenckhahn D, Adamson RH, Barth H, Curry FE. cAMP protects endothelial barrier functions by preventing Rac-1 inhibition. Am J Physiol Heart Circ Physiol. 2004;287:H2427-33.
19. Kobayashi K, Tsubosaka Y, Hori M, Narumiya S, Ozaki H, Murata T. Prostaglandin D2-DP signaling promotes endothelial barrier function via the cAMP/PKA/Tiam1/Rac1 pathway. Arterioscler Thromb Vasc Biol. 2013;33:565-71.
20. Fukuhara S, Sakurai A, Sano H, Yamagishi A, Somekawa S, Takakura N, et al. Cyclic AMP potentiates vascular endothelial cadherin-mediated cell-cell contact to enhance

endothelial barrier function through an Epac-Rap1 signaling pathway. Mol Cell Biol. 2005;25:136-46.

21. Adamson RH, Ly JC, Sarai RK, Lenz JF, Altangerel A, Drenckhahn D, et al. Epac/Rap1 pathway regulates microvascular hyperpermeability induced by PAF in rat mesentery. Am J Physiol Heart Circ Physiol. 2008;294:H1188-96.
22. Brown EB, Campbell RB, Tsuzuki Y, Xu L, Carmeliet P, Fukumura D, et al. In vivo measurement of gene expression, angiogenesis and physiological function in tumors using multiphoton laser scanning microscopy. Nat Med. 2001;7:864-8.
23. Harney AS, Arwert EN, Entenberg D, Wang Y, Guo P, Qian BZ, et al. Real-time imaging reveals local, transient vascular permeability, and tumor cell intravasation stimulated by TIE2hi macrophage-derived VEGFA. Cancer Discov. 2015;5:932-43.
24. Hirata E, Girotti MR, Viros A, Hooper S, Spencer-Dene B, Matsuda M, et al. Intravital imaging reveals gow BRAF inhibition generates drugtolerant microenvironments with high integrin beta1/FAK signaling. Cancer Cell. 2015;27:574-88.
25. Nobis M, McGhee EJ, Morton JP, Schwarz JP, Karim SA, Quinn J, et al. Cancer ResIntravital FLIM-FRET imaging reveals dasatinib-induced spatial control of Src in pancreatic cancer. Cancer research. 2013;73:4674-86.
26. Kamioka Y, Sumiyama K, Mizuno R, Sakai Y, Hirata E, Kiyokawa E, et al. Live imaging of protein kinase activities in transgenic mice expressing FRET biosensors. Cell Strcuture and Function. 2012;37:65-73.
27. Johnsson AK, Dai Y, Nobis M, Baker MJ, McGhee EJ, Walker S, et al. The Rac-FRET mouse reveals tight spatiotemporal control of Rac activity in primary cells and tissues. Cell Rep. 2014;6:1153-64.
28. Hida K, Hida Y, Amin DN, Flint AF, Panigrahy D, Morton CC, et al. Tumor-associated endothelial cells with cytogenetic abnormalities. Cancer research. 2004;64:8249-55.
29. Ponsioen B, Zhao J, Riedl J, Zwartkruis F, van der KG, Zaccolo M, et al. Detecting cAMP-induced Epac activation by fluorescence resonance energy transfer: Epac as a novel cAMP indicator. EMBO Rep. 2004;5:1176-80.

30. Akagi T, Shishido T, Murata K, Hanafusa H. v-Crk activates the phosphoinositide 3-kinase/AKT pathway in transformation. Proc Natl Acad Sci U S A. 2000;97:7290-5.
31. Aoki K, Matsuda M. Visualization of small GTPase activity with fluorescence resonance energy transfer-based biosensors. Nat Protoc. 2009;4:1623-31.
32. Mizuno R, Kamioka Y, Kabashima K, Imajo M, Sumiyama K, Nakasho E, et al. In vivo imaging reveals PKA regulation of ERK activity during neutrophil recruitment to inflamed intestines. J Exp Med. 2014;211:1123-36.
33. Komatsu N, Aoki K, Yamada M, Yukinaga H, Fujita Y, Kamioka Y, et al. Development of an optimized backbone of FRET biosensors for kinases and GTPases. Mol Biol Cell. 2011;22:4647-56.
34. Surapisitchat J, Beavo JA. Regulation of endothelial barrier function by cyclic nucleotides: the role of phosphodiesterases. Handb Exp Pharmacol. 2011:193-210.
35. Polverino A, Coxon A, Starnes C, Diaz Z, DeMelfi T, Wang L, et al. AMG 706, an oral, multikinase inhibitor that selectively targets vascular endothelial growth factor, platelet-derived growth factor, and kit receptors, potently inhibits angiogenesis and induces regression in tumor xenografts. Cancer research. 2006;66:8715-21.
36. Birukova AA, Burdette D, Moldobaeva N, Xing J, Fu P, Birukov KG. Rac GTPase is a hub for protein kinase A and Epac signaling in endothelial barrier protection by cAMP. Microvasc Res. 2010;79:128-38.
37. Ferrara N, Gerber HP, LeCouter J. The biology of VEGF and its receptors. Nat Med. 2003;9:669-76.
38. Xiong Y, Huo Y, Chen C, Zeng H, Lu X, Wei C, et al. Vascular endothelial growth factor (VEGF) receptor-2 tyrosine 1175 signaling controls VEGF-induced von Willebrand factor release from endothelial cells via phospholipase C-gamma 1- and protein kinase A-dependent pathways. J Biol Chem. 2009;284:23217-24.
39. Hudson N, Powner MB, Sarker MH, Burgoyne T, Campbell M, Ockrim ZK, et al. Differential apicobasal VEGF signaling at vascular blood-neural barriers. Dev Cell. 2014;30:541-52.

40. Kim C, Vigil D, Anand G, Taylor SS. Structure and dynamics of PKA signaling proteins. Eur J Cell Biol. 2006;85:651-4.

41. Kidoya H, Kunii N, Naito H, Muramatsu F, Okamoto Y, Nakayama T, et al. The apelin/APJ system induces maturation of the tumor vasculature and improves the efficiency of immune therapy. Oncogene. 2012;31:3254-64.

42. Chae SS, Paik JH, Furneaux H, Hla T. Requirement for sphingosine 1-phosphate receptor-1 in tumor angiogenesis demonstrated by in vivo RNA interference. J Clin Invest. 2004;114:1082-9.

43. Gratton JP, Lin MI, Yu J, Weiss ED, Jiang ZL, Fairchild TA, et al. Selective inhibition of tumor microvascular permeability by cavtratin blocks tumor progression in mice. Cancer Cell. 2003;4:31-9.

44. Turley RS, Fontanella AN, Padussis JC, Toshimitsu H, Tokuhisa Y, Cho EH, et al. Bevacizumab-induced alterations in vascular permeability and drug delivery: a novel approach to augment regional chemotherapy for in-transit melanoma. Clin Cancer Res. 2012;18:3328-39.

45. Bain J, Plater L, Elliott M, Shpiro N, Hastie CJ, McLauchlan H, et al. The selectivity of protein kinase inhibitors: a further update. Biochem J. 2007;408:297-315.

FIGURE LEGENDS

Figure 1. In vivo imaging of FRET mice visualized PKA activities in the endothelial cells within tumor tissue and subcutaneous tissue.

(A) Experimental schemes: (1) Colon-38 colon cancer cells expressing the Keima fluorescent protein were injected subcutaneously into PKAchu mice, which expressed a cytoplasmic FRET biosensor for PKA. (2) After the cancer cells had grown to visible size, intratumoral or subcutaneous (S.C.) blood vessels were observed by the skin-flap method under an inverted two-photon excitation microscope. (3) If necessary, drugs were administrated intravenously (I.V.) during imaging.

(B) Tumor tissue and subcutaneous tissue were imaged for collagen fiber (second harmonic, blue), host cells (YFP, green), and Colon-38 tumor cells (Keima, red). The blood vessels are marked with "V's". The scale bar represents 50 μm.

(C) Corresponding images of FRET/CFP, representing PKA activity in the host cells of the regions shown by white boxes in panel (B). The FRET/CFP images are shown in intensity-modulated display (IMD) mode with a 32-intensity in 8-ratio (0.8 – 1.8). Arrowheads, arrows and L indicate endothelial cells, platelets and the luminal space of blood vessels, respectively. The scale bar represents 20 μm.

(D) The tumor tissue was immunostained for GFP (green) and CD31 (red). Arrowheads show GFP-positive endothelial cells that formed the inner cellular lining of intratumoral blood vessels (V). Asterisks indicate GFP-negative cancer cells. Nuclei were stained with Hoechst (blue). The scale bar represents 50 μm.

Figure 2. PKA activity was lower in the intratumoral endothelial cells than the subcutaneous endothelial cells.

(A) Tumor-bearing mice (TBM) were prepared as in Fig. 1. Upper panels: Tumor or normal tissues were imaged for collagen fiber (second harmonic, blue), host cells (YFP, green), and tumor cells (Keima, red). Blood vessels are marked with a "V". Lower panels: Corresponding images of FRET/CFP, representing PKA activity in the host cells. The tumor cells used here

were Colon-38 colon cancer cells, Panc-02 pancreatic cancer cells, B16-F10 melanoma cells, and 3LL lung cancer cells (n > 3 mice for each). In subcutaneous arteriole, perictyes could also be observed (arrows). The scale bar represents 20 μm.

(B) Endothelial cells were randomly selected and examined for their PKA activity. Results obtained from at least three mice are combined. Black dots and red bars indicate the PKA activity in each endothelial cell (n =17-40 in each cell) and the mean ± SD, respectively. Differences from normal endothelial cells were evaluated by one-way ANOVA with Tukey post hoc analysis: *P < 0.05; ***P < 0.001. Images of all endothelial cells except those of intratumoral endothelial cells were pooled and used as the reference.

(C) FRET/CFP of normal and tumor endothelial cells in transgenic mice expressing the negative control FRET biosensor (PKA-NC). Results obtained from three mice are combined. Black dots and red bars indicate the FRET/CFP in each endothelial cell (n =22-24 in each cell) and the mean ± SD, respectively. No significant difference in FRET/CFP was observed. n.s., not significant (Student's *t*-test).

Figure 3. Intratumoral and subcutaneous endothelial cells exhibited similar ERK activity.

Tumor-bearing mice (TBM) were prepared as in Fig. 1 using Eisuke mice, which express a FRET biosensor for ERK. (A) Upper panels: Colon-38 tumor tissue and subcutaneous tissue were imaged for collagen fiber (second harmonic, blue), host cells (YFP, green), and tumor cells (Keima, red). Blood vessels are indicated with a "V". Lower panels: Corresponding images of FRET/CFP, representing ERK activity in the host cells (n = 3 mice for each). The scale bar represents 50 μm.

(B) Basal ERK activities of normal and tumor endothelial cells. Endothelial cells were randomly selected in the CFP images and examined for their ERK activity in the corresponding FRET/CFP ratio image. Results obtained from three mice are combined. Black dots and red bars indicate the ERK activity in each endothelial cell (n =21-24 in each cell) and the mean ± SD, respectively. n.s., not significant (one-way ANOVA).

Figure 4. dbcAMP reduced tumor vascular permeability.

(A) Experimental scheme for a modified Miles assay: (1) Cancer cells were injected subcutaneously into C57BL/6 Jcl mice. (2) Vehicles or drugs were intravenously administrated with Evans blue (50 mg/kg). Two hours later, mice were sacrificed for the examination of Evans blue extravasation.

(B) PBS or dbcAMP (50 or 100 mg/kg) was injected to examine the Evans blue extravasation. At least three mice were examined in each group. Data are represented as the mean ± SD (n =5-14 in each tissue). Differences were evaluated by Student's *t*-test: **P < 0.01; ***P < 0.001.

(C) Time-lapse FRET images of the tumor endothelial cells in the PKAchu mice bearing Colon-38 tumors. A vehicle (PBS) or dbcAMP (50 mg/kg) was injected intravenously at 0 min. Arrowheads and L indicate endothelial cells and the luminal space of blood vessels, respectively. The scale bar represents 10 μm.

(D) PKA activities in the intratumoral and subcutaneous endothelial cells. FRET images were acquired 16 min after vehicle (PBS) or dbcAMP injection (50 mg/kg). Three mice were analyzed for each condition (n =7-10 in each cell). Endothelial cells were randomly selected and examined for their PKA activity. Data are represented as the PKA activity (FRET/CFP) normalized to the respective mean values before drug injection. Bars are the mean ± SD. Differences from the vehicle group were evaluated by Student's *t*-test. **P < 0.01; ***P<0.001.

Figure 5. Activation of PKA or Epac/cAMP-GEF reduced tumor vascular permeability.

Mice bearing Colon-38 tumors were treated with the PKA activator 6-Bnz or Epac/cAMP-GEF activator 007 (0, 10, 25 or 50 mg/kg) together with Evans blue. Tumors and skin were excised 2 hr after administration for the analysis of Evans blue extravasation. At least three mice were examined in each group. Data are represented as the mean ± SD (n =6-14 in each tissue). Differences from the non-treated group were evaluated by Student's *t*-test: *P < 0.05; **P < 0.01.

Figure 6. The VEGFR inhibitor Motesanib reduced the tumor vascular permeability and this reduction was mediated by endothelial PKA activation.

(A) Tumor-bearing mice were treated with vehicle (saline containing 5% DMSO) or Motesanib (50 mg/kg) together with Evans blue. The tumors and skins were excised 2 hr after administration and Evans blue extravasation was quantified and expressed as ng of dye/mg of tissue (ng/mg tissue) ($n \geq 3$). Data are represented as the mean ± SD (n =5-8 in each tissue). Differences from the vehicle group were evaluated by Student's *t*-test: ***P < 0.001. The scale bar represents 10 mm.

(B and C) PKA or ERK activities in the intratumoral and subcutaneous endothelial cells were imaged in the PKAchu mice or Eisuke mice bearing Colon-38 tumors as in Fig. 1. FRET images were acquired 26 min after the vehicle or Motesanib injection (50 mg/kg) (N=3). Endothelial cells were randomly selected and examined for their PKA or ERK activity. Data are represented as the activity (FRET/CFP) normalized to the respective mean values before drug injection. Bars are the mean ± SD (n =6-12 in each cell). Differences from the vehicle group were evaluated by Student's *t*-test: ***P < 0.001. n.s., not significant by Student's *t*-test.

Figure 7. VEGF enhanced vascular permeability and decreased PKA activity in the subcutaneous endothelial cells.

(A) Extravasation of Evans blue in skin was quantified 30 min after subcutaneous injection of PBS (vehicle) or VEGF into C57BL/6N Jcl mice. The mean ± SD values are shown (n =3 in each tissue). Differences from the vehicle group were evaluated by Student's *t*-test: *P < 0.05. The photographs on the bottom indicate dye extravasation of Evans blue in skin.

(B) PKA activity in the subcutaneous endothelial cells was visualized with PKAchu mice as in Fig. 1. Mice were treated with PBS or VEGF for 30 min before acquisition of the images. The scale bar represents 10 μm.

(C) Endothelial cells were randomly selected and examined for their PKA activity (N = 3). Black dots and red bars indicate the PKA activity in each endothelial cell (n =27-29 in each

cell) and the mean ± SD, respectively. Differences from the vehicle group (PBS) were evaluated by Student's *t*-test: **P < 0.01.

(D-F) Timelapse FRET images of HUVEC expressing the PKA biosensor. At 0 min, 50 ng/ml of VEGF164 or PBS was added to the cells and imaged every 4 min for 1 h. The whole viewfield images (D) and images of a representative cell (E) are shown. The scale bar represents 10 μm. The experiment was repeated three times with similar results. The normalized PKA activity (FRET/CFP) was quantified at 32 min for 18 cells randomly selected from each of the three different experiments (F). Bars are the mean ± SD. Differences from the vehicle group were evaluated by Student's t-test. ***P<0.001.

Figure 1

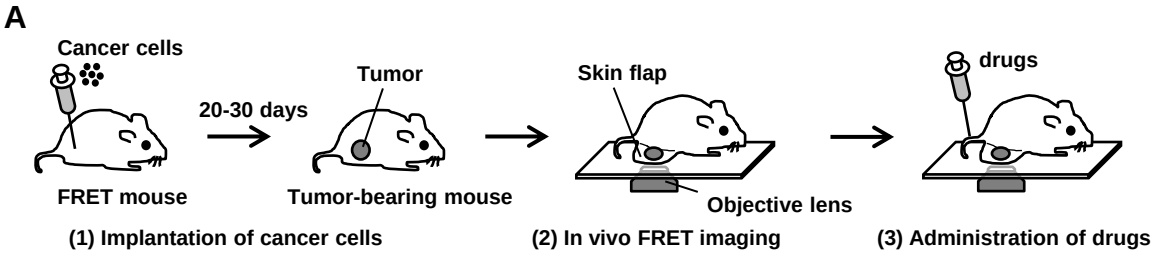
A
Cancer cells
FRET mouse
20-30 days
Tumor
Tumor-bearing mouse
Skin flap
Objective lens
drugs
(1) Implantation of cancer cells
(2) In vivo FRET imaging
(3) Administration of drugs

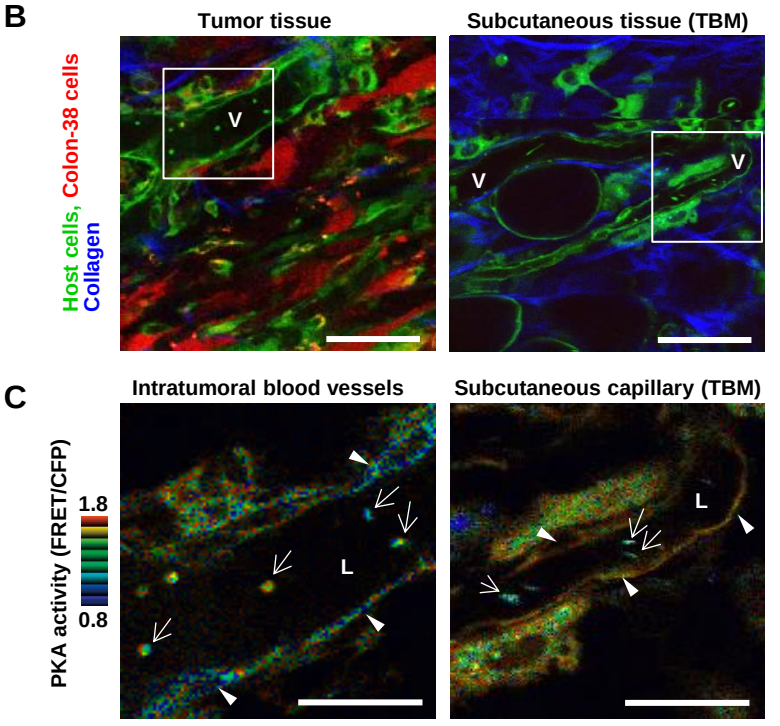
B
Tumor tissue
Subcutaneous tissue (TBM)
Host cells, Colon-38 cells
Collagen
V
C
Intratumoral blood vessels
Subcutaneous capillary (TBM)
PKA activity (FRET/CFP)
1.8
0.8
L

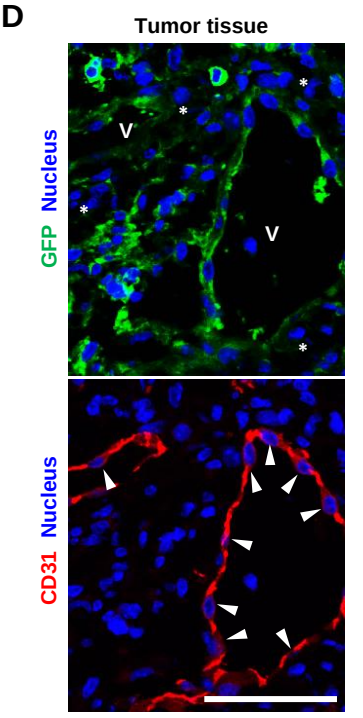
D
Tumor tissue
GFP Nucleus
CD31 Nucleus
V
*

Figure 2

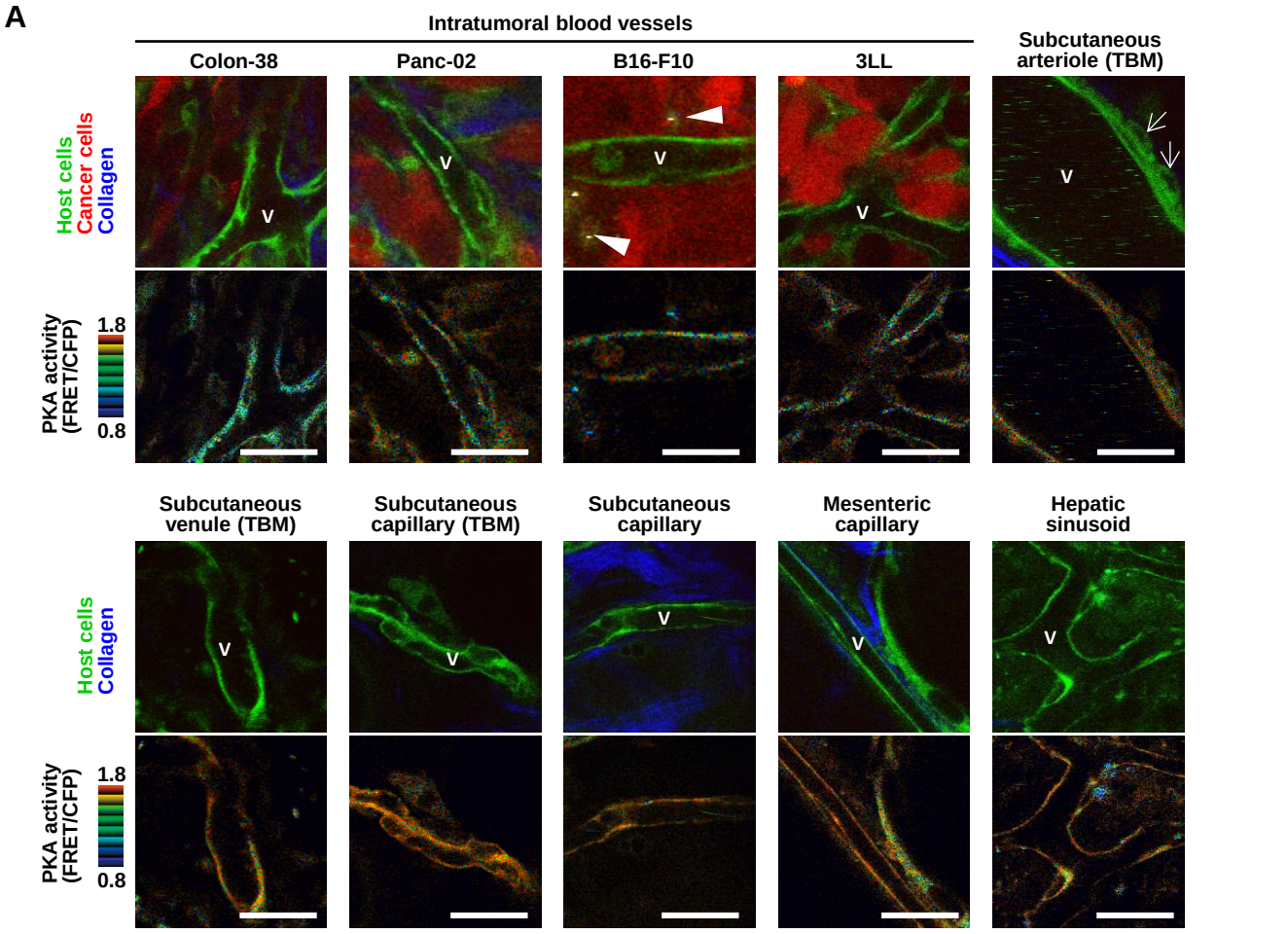
A
Intratumoral blood vessels
Colon-38
Panc-02
B16-F10
3LL
Subcutaneous arteriole (TBM)
Host cells
Cancer cells
Collagen
PKA activity (FRET/CFP)
1.8
0.8
V
Subcutaneous venule (TBM)
Subcutaneous capillary (TBM)
Subcutaneous capillary
Mesenteric capillary
Hepatic sinusoid

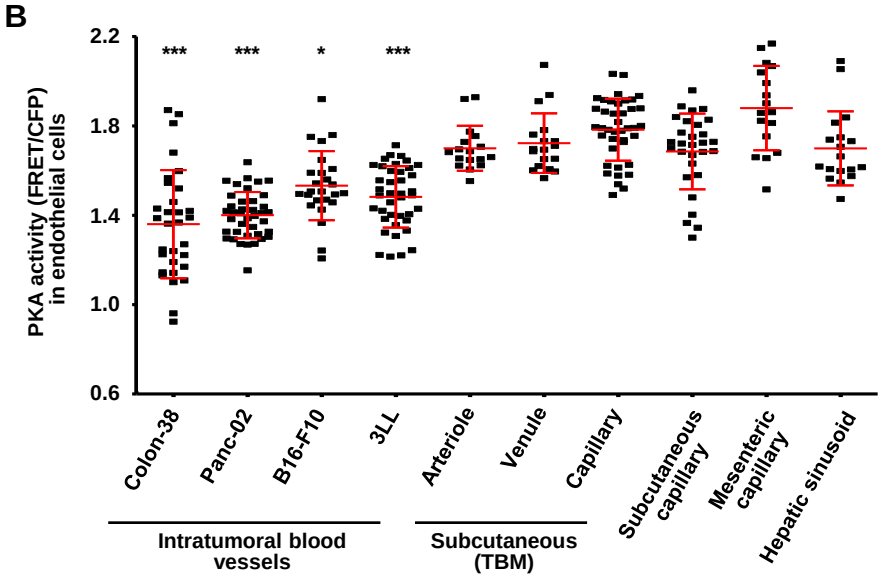
B
PKA activity (FRET/CFP) in endothelial cells
2.2
1.8
1.4
1.0
0.6
***
***
*
***
Colon-38
Panc-02
B16-F10
3LL
Arteriole
Venule
Capillary
Subcutaneous capillary
Mesenteric capillary
Hepatic sinusoid
Intratumoral blood vessels
Subcutaneous (TBM)

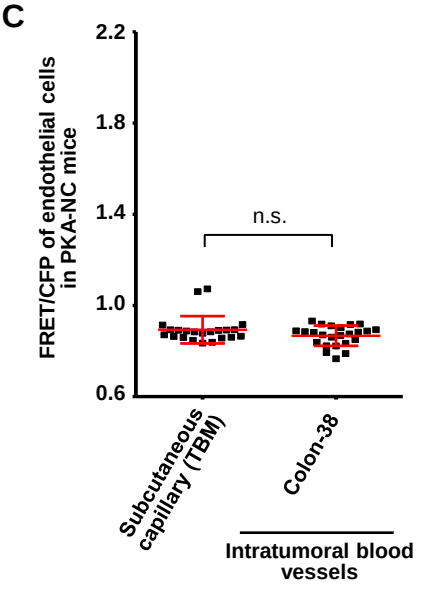
C
FRET/CFP of endothelial cells in PKA-NC mice
2.2
1.8
1.4
1.0
0.6
n.s.
Subcutaneous capillary (TBM)
Colon-38
Intratumoral blood vessels

Figure 3

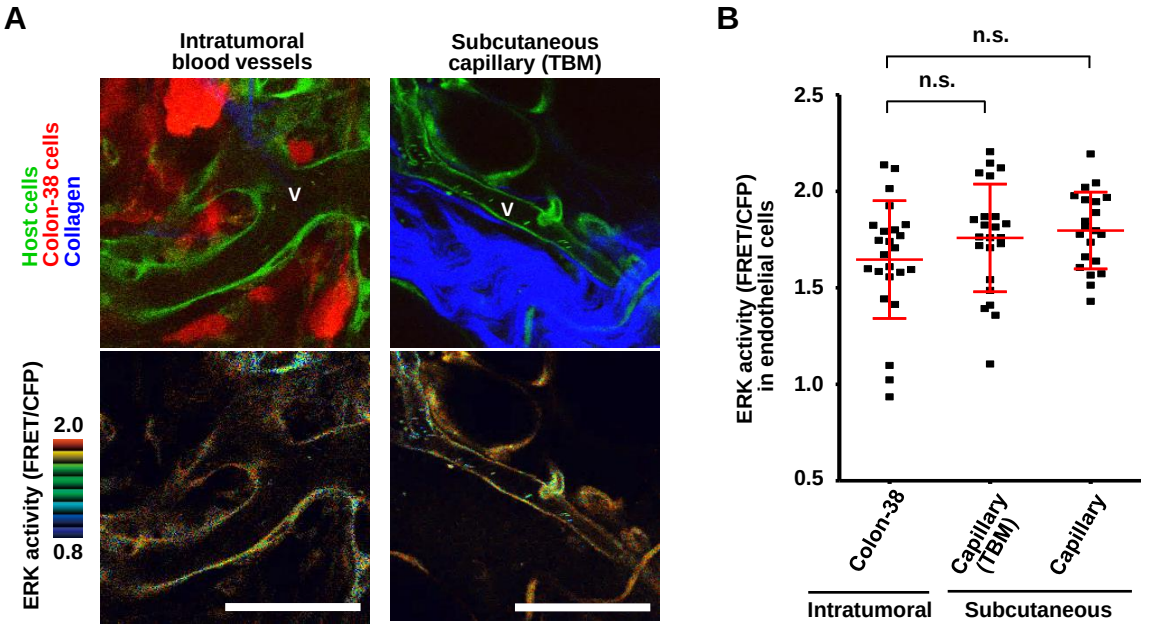
A
Intratumoral blood vessels
Subcutaneous capillary (TBM)
Host cells
Colon-38 cells
Collagen
V
V
ERK activity (FRET/CFP)
2.0
0.8
B
n.s.
n.s.
ERK activity (FRET/CFP) in endothelial cells
2.5
2.0
1.5
1.0
0.5
Colon-38
Capillary (TBM)
Capillary
Intratumoral
Subcutaneous

Figure 4

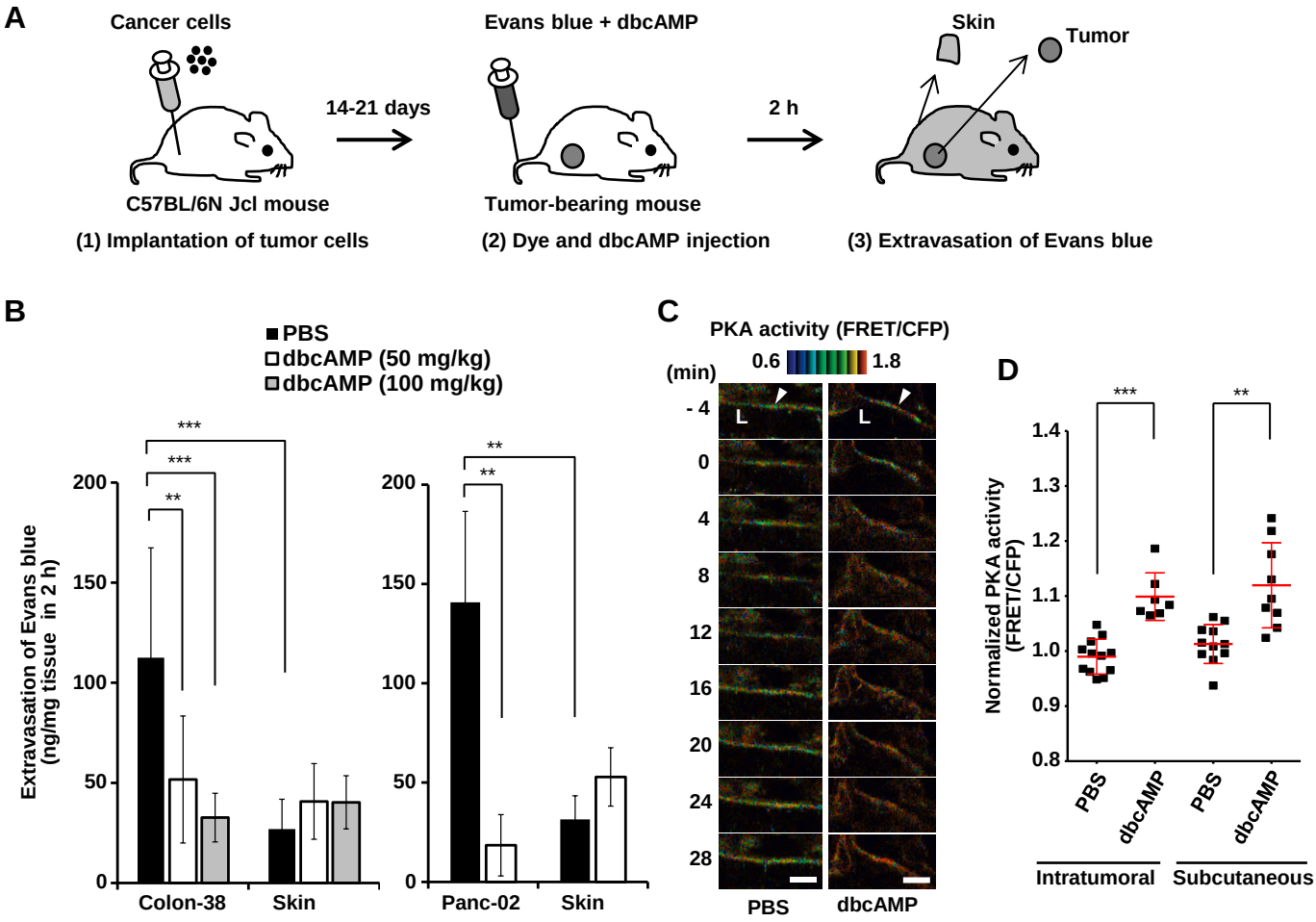
A
Cancer cells
14-21 days
Evans blue + dbcAMP
2 h
Skin
Tumor
C57BL/6N Jcl mouse
Tumor-bearing mouse
(1) Implantation of tumor cells
(2) Dye and dbcAMP injection
(3) Extravasation of Evans blue
B
PBS
dbcAMP (50 mg/kg)
dbcAMP (100 mg/kg)
Extravasation of Evans blue (ng/mg tissue in 2 h)
Colon-38
Skin
Panc-02
Skin
C
PKA activity (FRET/CFP)
(min)
0.6
1.8
L
PBS
dbcAMP
D
Normalized PKA activity (FRET/CFP)
PBS
dbcAMP
PBS
dbcAMP
Intratumoral
Subcutaneous

Figure 5

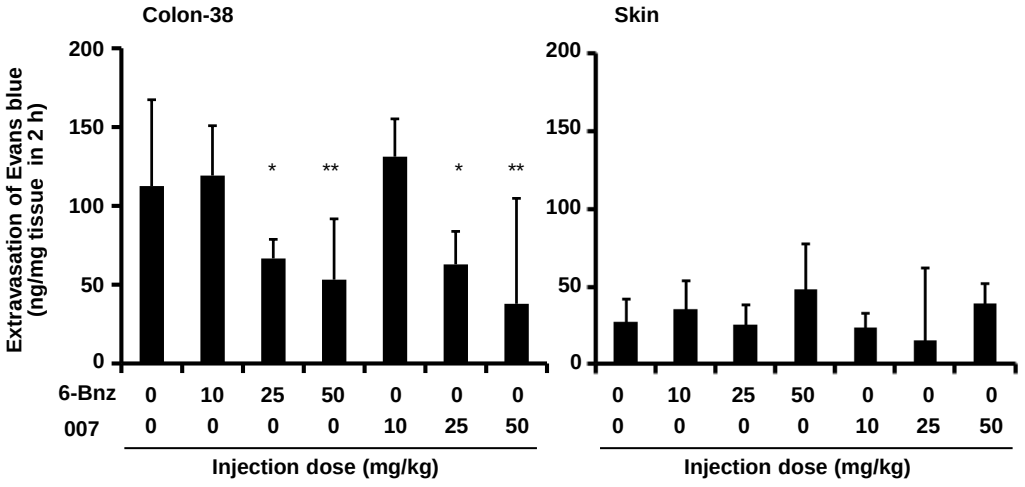
Colon-38
Skin
Extravasation of Evans blue (ng/mg tissue in 2 h)
200
150
100
50
0
*
**
*
**
6-Bnz
007
0 10 25 50 0 0 0
0 0 0 0 10 25 50
Injection dose (mg/kg)
Injection dose (mg/kg)

Figure 6

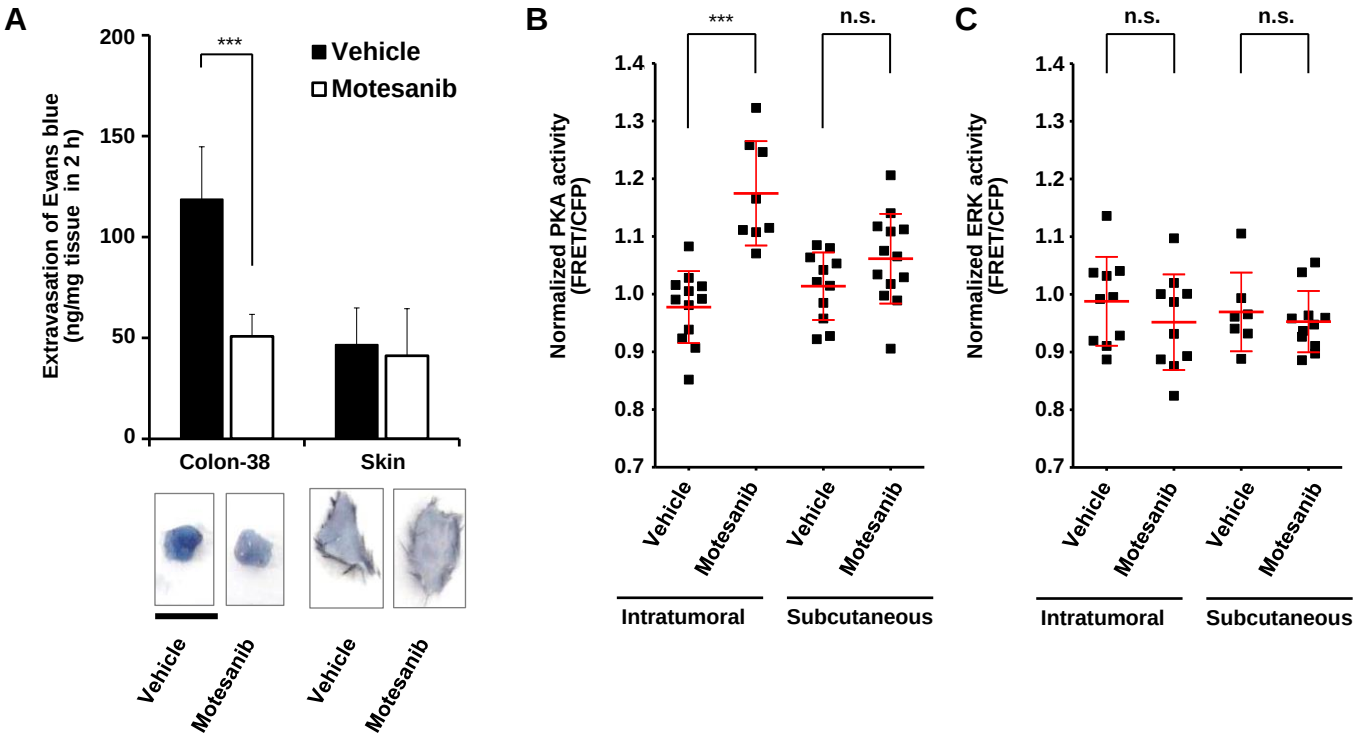
A
Extravasation of Evans blue (ng/mg tissue in 2 h)
200
150
100
50
0
***
Vehicle
Motesanib
Colon-38
Skin
Vehicle
Motesanib
Vehicle
Motesanib
B
Normalized PKA activity (FRET/CFP)
1.4
1.3
1.2
1.1
1.0
0.9
0.8
0.7
***
n.s.
Vehicle
Motesanib
Vehicle
Motesanib
Intratumoral
Subcutaneous
C
Normalized ERK activity (FRET/CFP)
1.4
1.3
1.2
1.1
1.0
0.9
0.8
0.7
n.s.
n.s.
Vehicle
Motesanib
Vehicle
Motesanib
Intratumoral
Subcutaneous

Figure 7

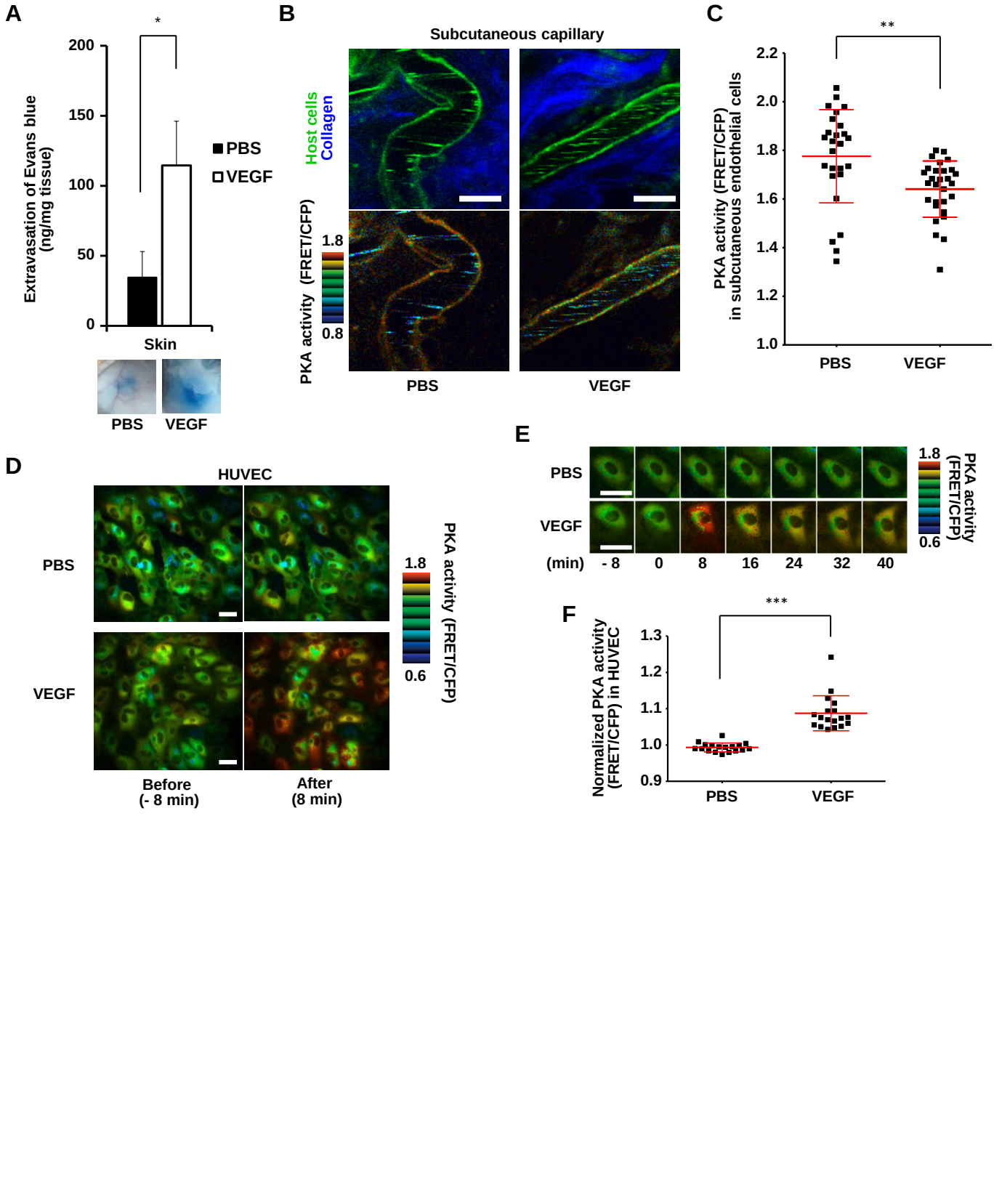
A
*
200
150
100
50
0
Extravasation of Evans blue (ng/mg tissue)
PBS
VEGF
Skin
PBS
VEGF
B
Subcutaneous capillary
Host cells
Collagen
PKA activity (FRET/CFP)
1.8
0.8
PBS
VEGF
C
**
PKA activity (FRET/CFP) in subcutaneous endothelial cells
2.2
2.0
1.8
1.6
1.4
1.2
1.0
PBS
VEGF
D
HUVEC
PBS
VEGF
1.8
0.6
PKA activity (FRET/CFP)
Before (- 8 min)
After (8 min)
E
PBS
VEGF
1.8
0.6
PKA activity (FRET/CFP)
(min)
- 8
0
8
16
24
32
40
F
***
Normalized PKA activity (FRET/CFP) in HUVEC
1.3
1.2
1.1
1.0
0.9
PBS
VEGF

SUPPLEMENTARY MATERIALS AND METHODS

Two-photon excitation microscopy and image processing

We used an IR-cut filter, BA685RIF-3, two dichroic mirrors, DM505 and DM570, and four emission filters, FF01-425/30 (Semrock, Rochester, NY) for second harmonic generation (SHG) images, BA460–500 (Olympus) for CFP, BA520–560 (Olympus) for yellow fluorescent protein (YFP; i.e. FRET), and 645/60 (Chroma Technology Corp., Bellows Falls, VT) for Qtracker 655. The microscope was equipped with a two-channel GaAsP detector unit and two built-in photomultiplier tubes. FluoView software (Olympus) was used to control the microscope and to acquire images, which were saved in the multilayer 16-bit Tagged Image File Format.

In vivo observation of the vascular endothelial cells

The FRET efficiency, namely the activity of PKA or ERK, was represented by the FRET/CFP ratio image in intensity modulated display mode; eight colors from red to blue were used to represent the FRET/CFP ratio, and 32 grades of color intensity were used to represent the signal intensity of the CFP image. The warm and cold colors indicate high and low FRET efficiencies, respectively. The SHG signal was also imaged. Vascular endothelial cells could be distinguished from the other cell types by their characteristic morphology and location. The thin cells lined the interior surface of blood vessels.

SUPPLEMENTARY FIGURE LEGENDS

Figure S1. FRET biosensors detect protein kinase activities in vascular endothelial cells.

(A) Mode of action of the intramolecular FRET biosensor. Phosphorylation with PKA or ERK induces an interaction between the sensor and ligand domains, which serves to increase the FRET efficiency from CFP to YFP.

(B and C) Structure of the PKA or ERK biosensor consisting of YFPs (donor), a FHA1 or WW phosphopeptide binding domain (ligand domain), a 72-Gly linker (EV linker), a PKA or ERK substrate (sensor domain), CFPs (acceptor), and a nuclear export signal (NES). In the substrate peptide sequences, red letters indicate the phosphorylation site. Blue letters indicate amino-acid substitutions to increase the affinity to either the FHA1 or WW domain. Green letters indicate the docking site of the kinases.

(D) FRET images of the intratumoral blood vessels and subcutaneous capillaries in tumor-bearing FRET mice. Arrowheads, arrows and L indicate vascular endothelial cells, pericytes and the luminal space of blood vessels. Although pericytes were closely associated with the endothelial cells, the cells were distinguishable. The scale bar represents 50 μm.

(E) Z-stack images of intratumoral blood vessels. Before data acquisition, Z-stack imaging of blood vessels was performed to check for the presence of pericytes on endothelial cells. Such pericyte-covered endothelial cells were excluded when determining the FERT/CFP ratio. The arrow indicates pericytes on tumor endothelial cells. The scale bar represents 50 μm.

(F) Qtracker 655 vascular tracer was injected intravenously to check the vascular perfusion and the lining of endothelial cells. The tracer revealed that the endothelial cells of interest lined the functional blood vessels in living tumors.

(G) ROI measurement of vascular endothelial cells for FRET analysis. The scale bar represents 50 μm.

Figure S2. PKA biosensor specifically detects PKA activity.

(A) PKA activity in tumor tissue was visualized with PKAchu mice as in Fig. 1. Tumor tissues were treated with vehicle (5% DMSO/saline) or a PKA inhibitor (H89) for 30 min before acquisition of the images. Upper panels: Tumor tissues were imaged for collagen fiber (second harmonic, blue), host cells (YFP, green), and Colon-38 tumor cells (Keima, red). Blood vessels are marked with a "V". Lower panels: Corresponding images of FRET/CFP, representing PKA activity in the host cells. H89 treatment remarkably reduced the PKA activity of stromal cells (arrowheads).

(B) Extended images of FRET/CFP of the regions shown by white boxes in panel (D). Arrowheads and L indicate endothelial cells and the luminal space of blood vessels, respectively. The PKA activity in the intratumoral endothelial cells was decreased with H89, indicating the high specificity of the PKA biosensor. The scale bar represents 10 μm.

(C) Time-lapse FRET images of the tumor endothelial cells in the PKAchu mice bearing Colon-38 tumors. Vehicle (PBS), 6-Bnz (50 mg/kg) or 007 (50 mg/kg) was injected intravenously. FRET images were acquired 16 min after the drug injection. Three mice were analyzed independently in each group. In each mouse, endothelial cells were randomly selected in the CFP images and examined for their PKA activity in the corresponding FRET/CFP ratio image. Bars are the mean ± SD (n=9-11 in each group). Differences from the vehicle group were evaluated by Student's *t*-test: ***$P < 0.001$; n.s., not significant.

Figure S3. Motesanib suppresses the activity of VEGFR2 in tumor endothelial cells in vivo.

Tumor-bearing mice (TBM) were prepared as in Fig. 4. To assess the effect of Motesanib on VEGFR2 activity, Motesanib (50 mg/kg) or vehicle (5% DMSO) was injected intravenously into tumor-bearing C57BL/6N Jcl mice. Mice were subjected to 4% paraformaldehyde perfusion 2 hr after the drug injection and sacrificed. Immunohistochemistry of frozen tumor tissue was performed as described in Materials and Methods.

(A) The tumor tissue was immunostained for VEGFR2 (green) and CD31 (red). Arrowheads show the VEGFR2-positive endothelial cells of intratumoral blood vessels (V). Nuclei were stained with DAPI (blue). The scale bar represents 50 μm.

(B) CD31-positive endothelial cells were randomly selected and examined for their VEGFR2 fluorescent intensity in each image. Results obtained from three mice are combined. Data are the mean ± SD. Differences were evaluated by Student's *t*-test: n.s., not significant.

(C) The tumor tissue was immunostained for pVEGFR2 (green) and CD31 (red). Arrowheads show pVEGFR2-positive endothelial cells of intratumoral blood vessels (V). Nuclei were stained with DAPI (blue). The scale bar represents 50 μm.

(D) CD31-positive endothelial cells were randomly selected and examined for their pVEGFR2 fluorescent intensity in each image. Results obtained from three mice are combined. Data are the mean ± SD. Differences were evaluated by Student's *t*-test: ***P < 0.001.

These data shows that Motesanib suppresses the tyrosine kinase activity of VEGFR2 in tumor endothelial cells. VEGFR2 expression was not changed by 2 hr of Motesanib treatment.

Figure S4. VEGF activates ERK in tumor endothelial cells and HUVEC.

(A) ERK activities in the intratumoral and subcutaneous endothelial cells were imaged in the Eisuke mice bearing Colon-38 tumors as in Fig. 1. FRET images were

acquired 30 min after the PBS (vehicle) or VEGF injection (5 μg/mouse). Three mice were analyzed independently in each group. In each mouse, endothelial cells were randomly selected in the CFP images and examined for their ERK activity in the corresponding FRET/CFP ratio image. Data are the activity (FRET/CFP) normalized to the respective mean values before drug injection. Bars are the mean ± SD. Differences from the vehicle group were evaluated by Student's *t*-test: ***P < 0.001. n.s., not significant (Student's *t*-test). The data shows that VEGF activates ERK in tumor endothelial cells.

(B and C) Representative time-lapse FRET images of the tumor endothelial cells in the Eisuke mice bearing Colon-38 tumors. VEGF (5 μg/mouse) was injected intravenously at 0 min. After ca. 60 min, Motesanib (50 mg/kg) was injected intravenously. The scale bar represents 20 μm. Quantitative data represent the activity (FRET/CFP) normalized to the respective mean values before VEGF injection (C). These data confirm that Motesanib counteracts VEGF in tumor endothelial cells. Because the mouse moved at 60 min, images during the search for the original position could not be acquired until 80 min.

(D) HUVEC expressing the ERK biosensor were treated with PBS, VEGF (50 ng/mL), or PD0325901 (10 μM, MEK inhibitor). PD0325901 was used as a working control for the ERK biosensor. FRET images were acquired 12 min after the stimulation. HUVEC were randomly selected in the CFP images and examined for their ERK activity in the corresponding FRET/CFP ratio image. Black dots and red bars indicate the normalized ERK activity in each cell and the mean ± SD, respectively. Differences from the vehicle group (PBS) were evaluated by Student's *t*-test: ***P < 0.001, *P < 0.05.

Figure S5. VEGF increases in cAMP level in HUVEC, but not Hela cells.

(A) FRET images of HUVEC expressing the Epac-cAMP sensor. The cAMP level in HUVEC was visualized as in Fig. 7D. HUVEC were treated with PBS, VEGF (100 ng/mL), or Forskolin+ IBMX (positive control). The scale bar represents 20 μm.

(B) FRET images were acquired 36 min after the stimulation. HUVEC were randomly selected in the CFP images and examined for the cAMP level in the corresponding CFP/FRET ratio image. Black dots and red bars indicate the normalized cAMP level in each cell and the mean ± SD, respectively. Differences from the vehicle group (PBS) were evaluated by Student's *t*-test: ***P < 0.001. The data shows that VEGF increases in cAMP level in HUVEC, albeit markedly less than does Forskolin + IBMX treatment.

(C) FRET images of HeLa cells expressing the Epac-cAMP sensor. Epac activity in HeLa cells was visualized as in Fig. 7D. HeLa cells were treated with PBS, VEGF (100 ng/mL), or Forskolin and IBMX (positive control). The scale bar represents 20 μm.

(D) FRET images were acquired 36 min after the stimulation. HeLa cells were randomly selected in the CFP images and examined for the cAMP level in the corresponding CFP/FRET ratio image. Black dots and red bars indicate the normalized cAMP level and the mean ± SD, respectively. Differences from the vehicle group (PBS) were evaluated by Student's *t*-test: ***P < 0.001. The data shows that VEGF does not increase in cAMP level in HeLa cells.

Figure S6. Endothelial cells isolated from subcutaneous tissues exhibit phenotypes similar to the endothelial cells in vivo.

To isolate vascular endothelial cells from tumor tissue, a herpes simplex virus-thymidine kinase (HSV-TK) gene/ganciclovir (GCV) suicide gene system was used in this study. Colon-38 cells were infected with the HSV-TK gene by retroviral transduction and cloned, yielding cells highly sensitive to GCV (4 μg/ml). The colon38 cells expressing HSV-TK were injected subcutaneously into the flanks of PKAchu or

Eisuke mice. The grown tumor or skin was excised for isolation of tumor or normal endothelial cells, respectively. CD31-positive endothelial cells were isolated by MACS (Milteny) and grown in EGM-2MV medium. To remove tumor cells, GCV (4 μg/ml) was added to the culture medium.

(A) Isolated tumor and subcutaneous endothelial cells were immunostained with anti-CD31 antibody, an endothelial cell marker. The scale bar represents 100 μm. The cells were fixed with cold acetone and stained with anti-CD31 antibody conjugated with Alexa Fluor 594. DAPI was used to stain DNA. Fluorescent images were acquired with a confocal microscope (FV1000i; Olympus).

(B) PKA activity in the isolated tumor and subcutaneous endothelial cells was visualized with the PKA FRET biosensor AKAR3EV-NES. The scale bar represents 100 μm.

(C) Endothelial cells were randomly selected in the CFP images and examined for their PKA activity in the corresponding FRET/CFP ratio image. Black dots and red bars indicate the PKA activity in each endothelial cell and the mean ± SD, respectively. Differences were evaluated by Student's *t*-test: ***P < 0.001. The PKA activity of isolated subcutaneous endothelial cells was higher than that of isolated tumor endothelial cells.

(D) With cells expressing the PKA FRET biosensor, FRET images were acquired before (-4 min) and after (16 min) the VEGF stimulation (100 ng/mL). Black dots indicate the PKA activity in each endothelial cell. Differences were evaluated by Student's paired *t*-test: ***P < 0.001. The results showed a reduction of PKA activity under VEGF stimulation.

(E) The change of PKA activity under dbcAMP stimulation (1 mM) in tumor and subcutaneous endothelial cells. FRET images were acquired before (-4 min) and after (16 min) the stimulation. Black dots indicate the PKA activity in each endothelial cell.

Differences were evaluated by Student's paired *t*-test: **P < 0.01, *P < 0.05. The results showed that PKA was activated under dbcAMP stimulation.

(F) The change of ERK activity under VEGF stimulation (100 ng/mL) in tumor endothelial cells. FRET images were acquired before (-4 min) and after (8 min) the stimulation. Black dots indicate the ERK activity in the tumor endothelial cells. Differences were evaluated by Student's paired *t*-test: n.s., not significant. No VEGF-induced ERK activation was detected.

Figure S1

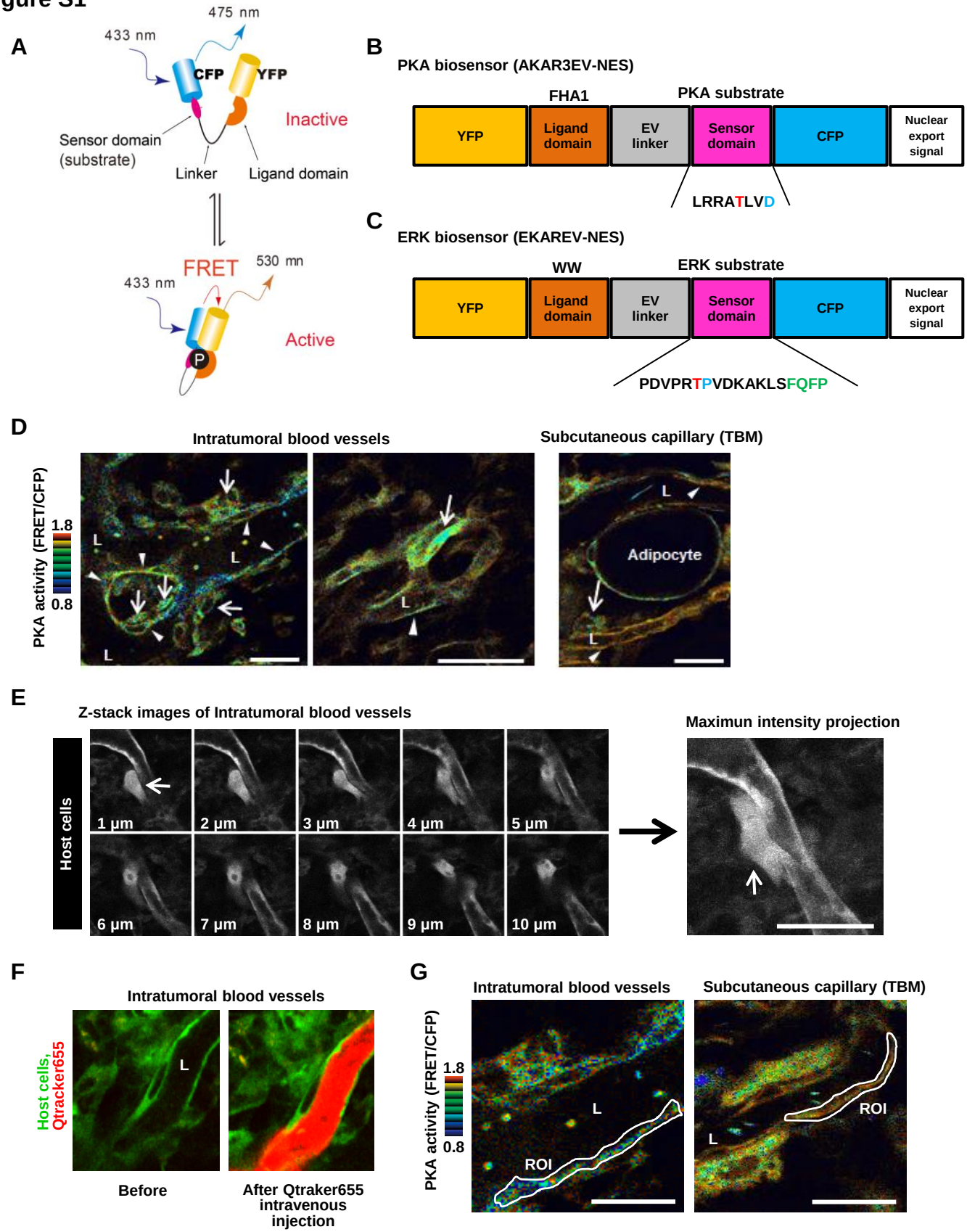
A
475 nm
433 nm
CFP
YFP
Inactive
Sensor domain (substrate)
Linker
Ligand domain
FRET
530 mn
433 nm
Active
P
B
PKA biosensor (AKAR3EV-NES)
FHA1
PKA substrate
YFP
Ligand domain
EV linker
Sensor domain
CFP
Nuclear export signal
LRRATLVD
C
ERK biosensor (EKAREV-NES)
WW
ERK substrate
YFP
Ligand domain
EV linker
Sensor domain
CFP
Nuclear export signal
PDVPRTPVDKAKLSFQFP
D
Intratumoral blood vessels
Subcutaneous capillary (TBM)
PKA activity (FRET/CFP)
1.8
0.8
L
Adipocyte
E
Z-stack images of Intratumoral blood vessels
Maximun intensity projection
Host cells
1 μm
2 μm
3 μm
4 μm
5 μm
6 μm
7 μm
8 μm
9 μm
10 μm
F
Intratumoral blood vessels
Host cells, Qtracker655
L
Before
After Qtraker655 intravenous injection
G
Intratumoral blood vessels
Subcutaneous capillary (TBM)
PKA activity (FRET/CFP)
1.8
0.8
L
ROI
L
ROI

Figure S2

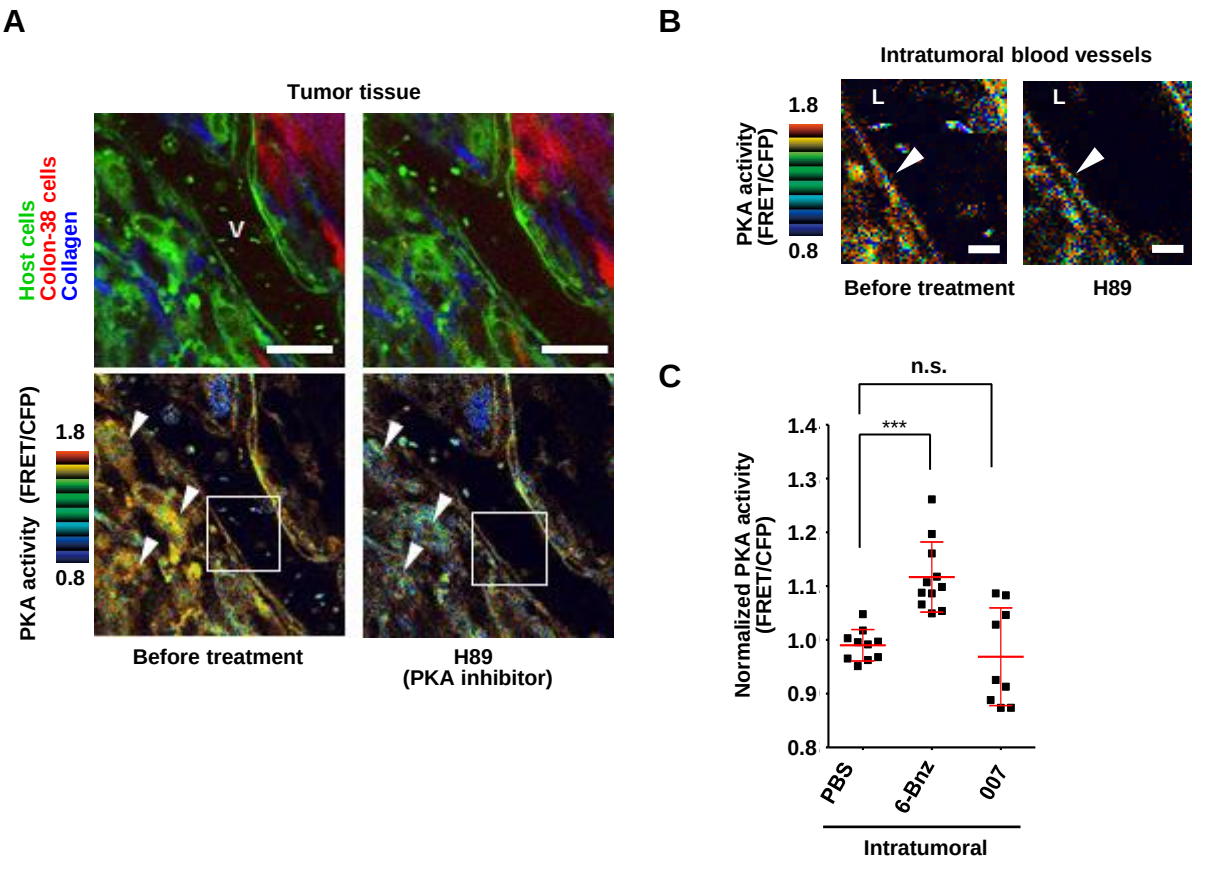
A
Tumor tissue
Host cells
Colon-38 cells
Collagen
V
PKA activity (FRET/CFP)
1.8
0.8
Before treatment
H89
(PKA inhibitor)
B
Intratumoral blood vessels
PKA activity
(FRET/CFP)
1.8
0.8
L
L
Before treatment
H89
C
n.s.
***
Normalized PKA activity
(FRET/CFP)
1.4
1.3
1.2
1.1
1.0
0.9
0.8
PBS
6-Bnz
007
Intratumoral

Figure S3

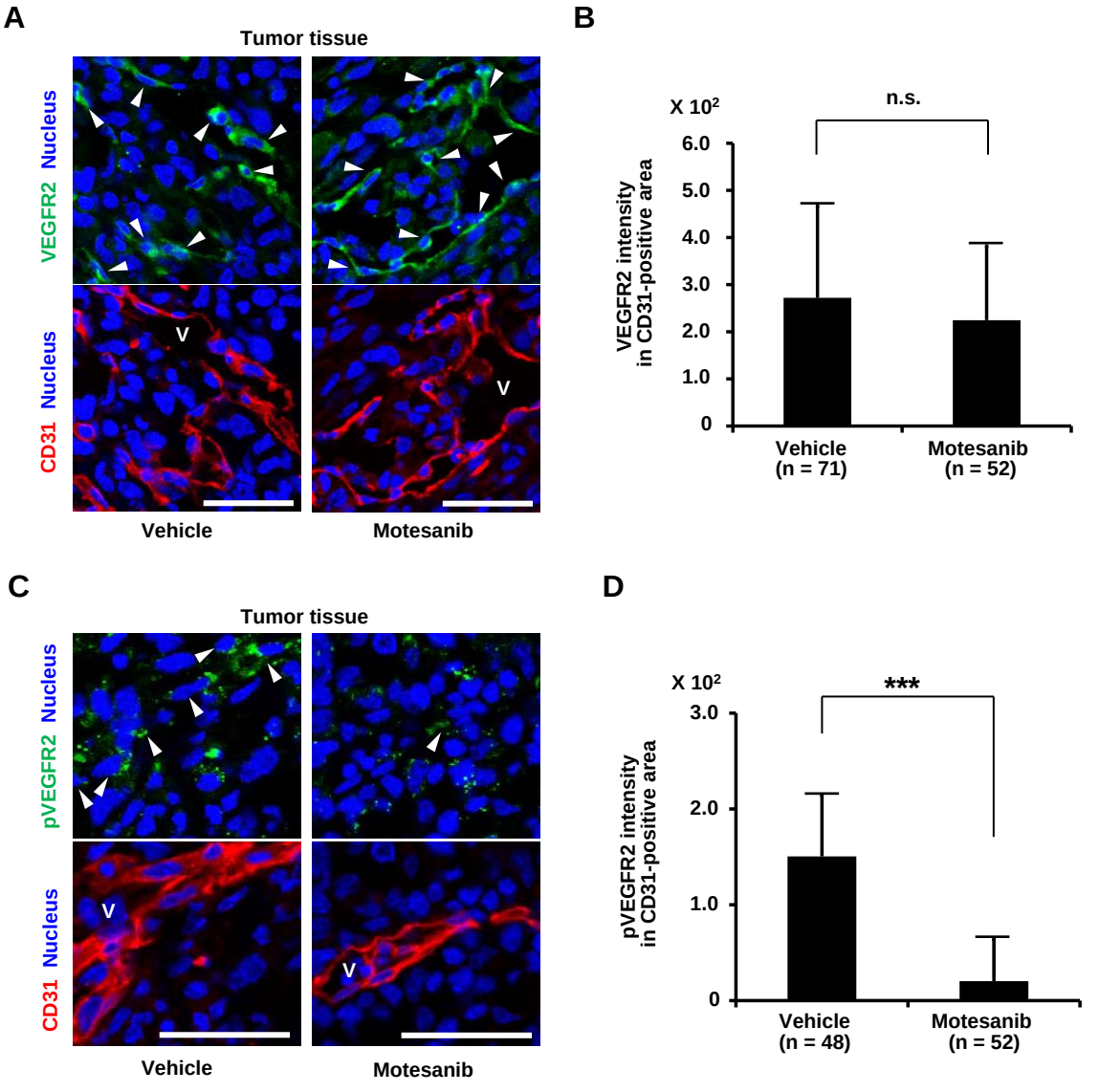
A
Tumor tissue
VEGFR2
Nucleus
CD31
Nucleus
V
V
Vehicle
Motesanib
B
X 10²
n.s.
VEGFR2 intensity in CD31-positive area
6.0
5.0
4.0
3.0
2.0
1.0
0
Vehicle (n = 71)
Motesanib (n = 52)
C
Tumor tissue
pVEGFR2
Nucleus
CD31
Nucleus
V
V
Vehicle
Motesanib
D
X 10²
***
pVEGFR2 intensity in CD31-positive area
3.0
2.0
1.0
0
Vehicle (n = 48)
Motesanib (n = 52)

Figure S4

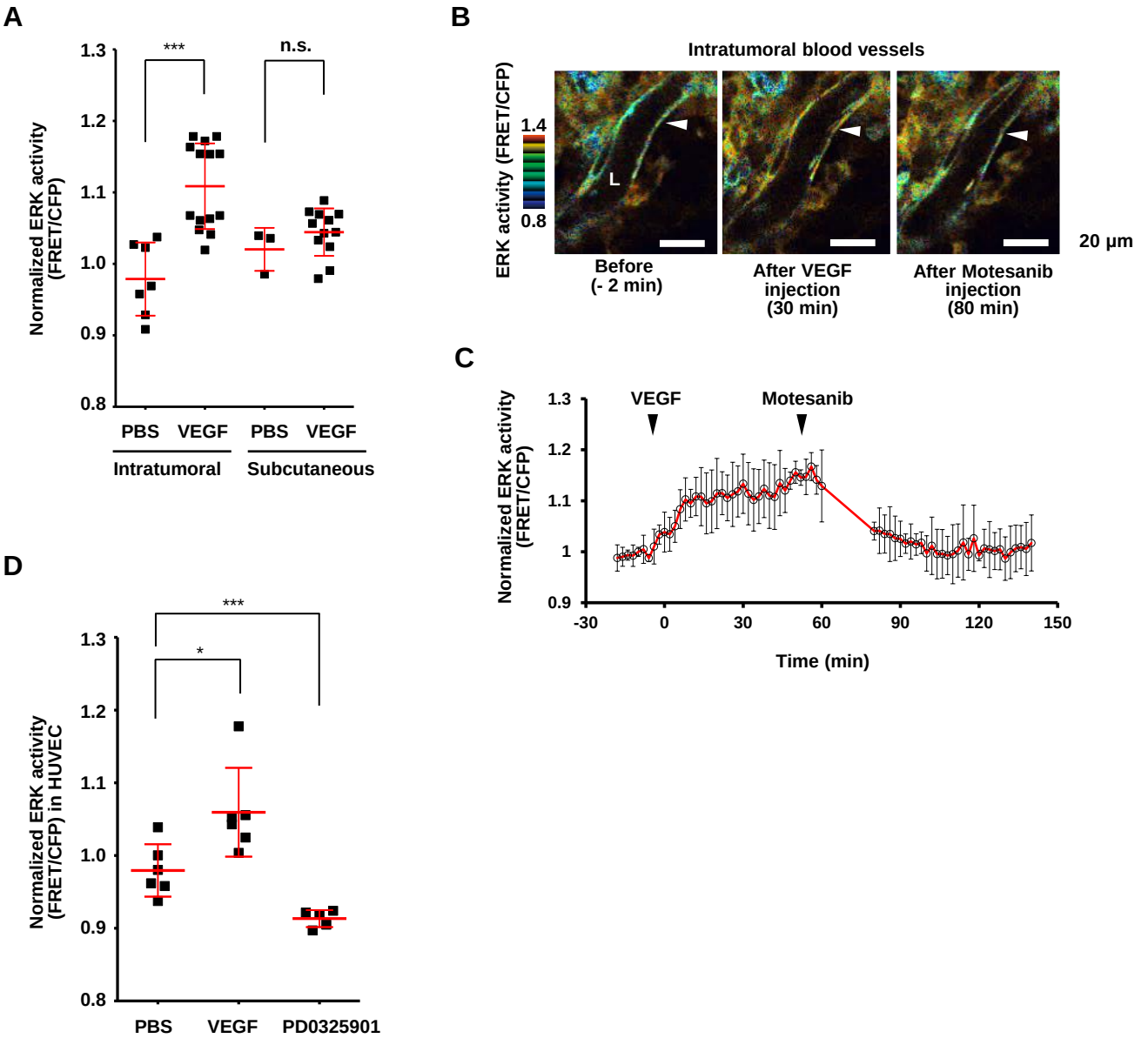
A
***
n.s.
Normalized ERK activity (FRET/CFP)
1.3
1.2
1.1
1.0
0.9
0.8
PBS
VEGF
PBS
VEGF
Intratumoral
Subcutaneous
B
Intratumoral blood vessels
ERK activity (FRET/CFP)
1.4
0.8
L
20 μm
Before (- 2 min)
After VEGF injection (30 min)
After Motesanib injection (80 min)
C
Normalized ERK activity (FRET/CFP)
VEGF
Motesanib
1.3
1.2
1.1
1
0.9
-30
0
30
60
90
120
150
Time (min)
D
***
*
Normalized ERK activity (FRET/CFP) in HUVEC
1.3
1.2
1.1
1.0
0.9
0.8
PBS
VEGF
PD0325901

Figure S5

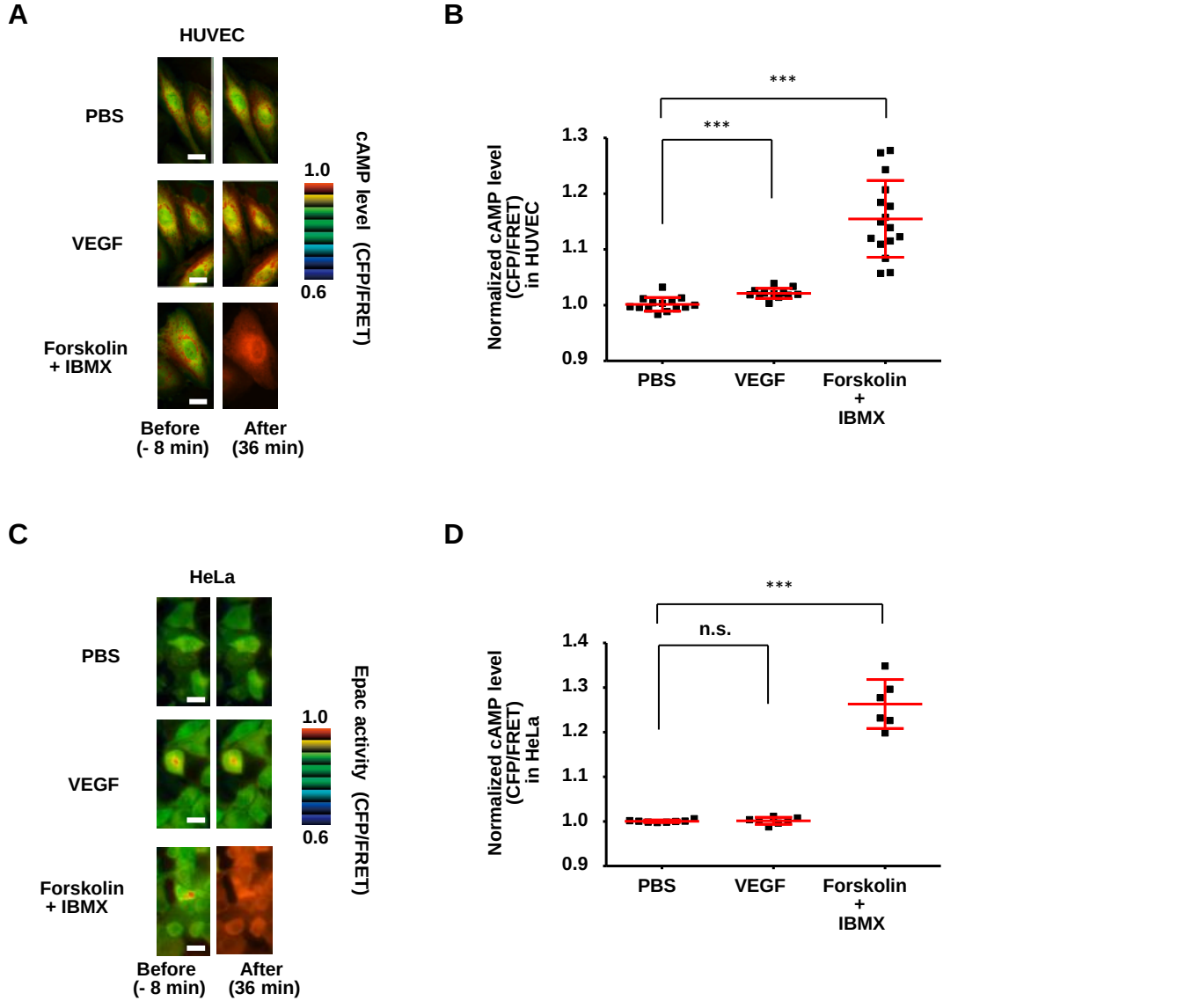
A
HUVEC
PBS
VEGF
Forskolin
+ IBMX
Before
(- 8 min)
After
(36 min)
1.0
0.6
cAMP level (CFP/FRET)
B
***
***
Normalized cAMP level
(CFP/FRET)
in HUVEC
1.3
1.2
1.1
1.0
0.9
PBS
VEGF
Forskolin
+
IBMX
C
HeLa
PBS
VEGF
Forskolin
+ IBMX
Before
(- 8 min)
After
(36 min)
1.0
0.6
Epac activity (CFP/FRET)
D
***
n.s.
Normalized cAMP level
(CFP/FRET)
in HeLa
1.4
1.3
1.2
1.1
1.0
0.9
PBS
VEGF
Forskolin
+
IBMX

Figure S6

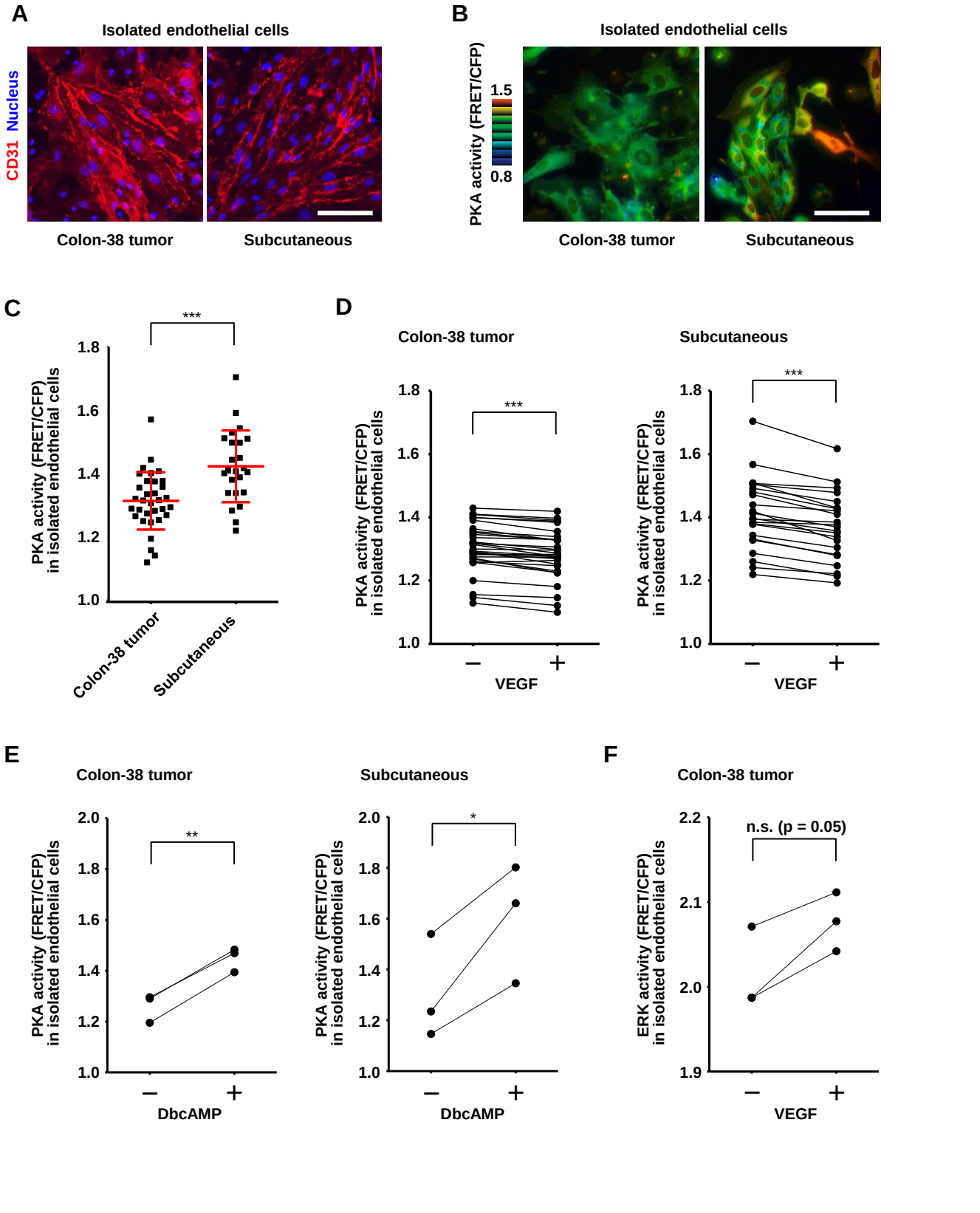
A
Isolated endothelial cells
CD31 Nucleus
Colon-38 tumor
Subcutaneous
B
Isolated endothelial cells
PKA activity (FRET/CFP)
1.5
0.8
Colon-38 tumor
Subcutaneous
C
***
PKA activity (FRET/CFP) in isolated endothelial cells
1.8
1.6
1.4
1.2
1.0
Colon-38 tumor
Subcutaneous
D
Colon-38 tumor
***
PKA activity (FRET/CFP) in isolated endothelial cells
1.8
1.6
1.4
1.2
1.0
–
+
VEGF
Subcutaneous
***
PKA activity (FRET/CFP) in isolated endothelial cells
1.8
1.6
1.4
1.2
1.0
–
+
VEGF
E
Colon-38 tumor
**
PKA activity (FRET/CFP) in isolated endothelial cells
2.0
1.8
1.6
1.4
1.2
1.0
–
+
DbcAMP
Subcutaneous
*
PKA activity (FRET/CFP) in isolated endothelial cells
2.0
1.8
1.6
1.4
1.2
1.0
–
+
DbcAMP
F
Colon-38 tumor
n.s. (p = 0.05)
ERK activity (FRET/CFP) in isolated endothelial cells
2.2
2.1
2.0
1.9
–
+
VEGF